**Institut für Hydrologie**
der Albert-Ludwigs-Universität Freiburg i. Br.

Daniel Thomas Radecke

# Effects of Groundwater Storage Properties on Low-Flow in a Pre Alpine Catchment

**Masterarbeit unter Leitung von Prof. Dr. Markus Weiler**

**Freiburg i. Br., Dezember 2011**

**Institut für Hydrologie**
der Albert-Ludwigs-Universität Freiburg i. Br.

Daniel Thomas Radecke

# Effects of Groundwater Storage Properties on Low-Flow in a Pre Alpine Catchment

**Referent: Prof. Dr. Markus Weiler**

**Korreferent: Prof. Dr. Jan Seibert**

**Masterarbeit unter Leitung von Prof. Dr. Markus Weiler**

**Freiburg i. Br., Dezember 2011**

# Danksagung

Dank für die für die Vergabe des Themas und für die inhaltlichen Anregungen gebührt Prof. Dr. Markus Weiler. Gedankt sei auch Prof. Dr. Jan Seibert für die Übernahme des Korreferats. Sehr dankbar bin ich auch für die Hilfestellungen und Anregungen in bezug auf meine Arbeit von Matthias Ritter, Anita Gundel und Till Volkmann.

Ich widme diese Arbeit meiner wunderbaren Georgia.

# Contents

# 1 Table of Variables

| Abbreviation | Description | Units |
|---|---|---|
| $b$ | Decay parameter of drainable porosity | $m$ |
| $\beta$ | Bypass power exponent | - |
| $d$ | Total layer thickness | $m$ |
| $\triangle$ | Gradient of saturated vapour pressure curve | $hPaK^{-1}$ |
| $E$ | Evaporation rate | $ms^{-1}$ |
| $EH$ | Net radiation equivalent | $ms^{-1}$ |
| $G$ | Gradient | - |
| $\gamma$ | Psychrometer constant | $hPaK^{-1}$ |
| $I$ | Effectively reflected radiation | $Wm^{-2}$ |
| $I_{in}$ | Infiltration rate | $m^3s^{-1}$ |
| $k_0$ | Saturated hydraulic conductivity at soil surface | $ms^{-1}$ |
| $k_{c,geo}$ | Constant saturated hydraulic conductivity of geological layer | $ms^{-1}$ |
| $k_s$ | Saturated hydraulic conductivity | $ms^{-1}$ |
| $l_a$ | Vapour pressure | $hPa$ |
| $l_s$ | Saturated vapour pressure | $hPa$ |
| $m$ | Shape parameter of hydraulic conductivity | $m$ |
| $n_0$ | Drainable porosity at soil surface | - |
| $n_d$ | Drainable porosity | - |
| $NSE$ | Nash-Sutcliffe Efficiency | - |
| $q$ | Flow rate | $m^3s^{-1}$ |
| $r$ | Albedo | % |
| $RE$ | Extraterrestial radiation | $Wm^{-2}$ |
| $RG$ | Global radiation | $Wm^{-2}$ |
| $RMSE$ | Root Mean Squared Error | - |
| $T$ | Transmittivity | $m^2s^{-1}$ |
| $\theta$ | Water content of the unsaturated zone | Vol. % |
| $V$ | Volume | $m^3$ |
| $v$ | Velocity | $ms^{-1}$ |
| $z$ | Depth into soil profile (positive downwards) | $m$ |

# Abstract

In this thesis runoff and isotope transport of the pre-alpine Rietholzbach catchment were modeled with respect to physically based soil and storage parameters in order to identify flow procecces and groundwater storage properties with a focus on low-flow characteristics. The modeling was performed by using the hillslope model HillVi. The model was well able to reproduce realistic values for runoff, especially under low-flow conditions. The isotope transport routine that has been implemented in this thesis enabled a calculation of mean transit times resulting in values of about 140 days to about 210 days depending on flow conditions. Based on the modeled storage properties an assessment of the Rietholzbach catchment's resilience to hydrological drought was made, according to which the Rietholzbach catchment is susceptible for droughts concerning runoff but only to a very limited extent with regard to groundwater availability.

*keywords: headwater catchment, groundwater, storages, transit time, low-flow*

# Zusammenfassung

In dieser Arbeit wurden Abfluss und Isotopentransport des Rietholzbach Einzugsgebietes unter Berücksichtigung von physikalisch basierten Boden- und Speicherparametern modelliert, um Fliessprozesse und Grundwasserspeichereigenschaften mit einem Fokus auf Niedrigwasserabfluss zu identifizieren. Die Modellierung wurde mit dem Hillslope Modell HillVi durchgeführt. Die bei dieser Arbeit eingeführte Routine für den Isotopentransport ermöglichte eine Berechnung von mittleren Verweilzeiten mit Ergebnissen zwsichen 140 und 210 Tagen je nach Abflussbedinungen. Basierend auf den modellierten Grundwasserspeichereigenschaften wurde eine Einschätzung der Resilienz zu Trockenheit des Rietholzbach Einzugsgebietes durchgeführt. Danach ist das Rietholzbach Einzusggebiet anfällig für Trockenheit in bezug auf den Abfluss aber nur sehr eingeschränkt in Bezug auf Grundwasserverfügbarkeit.

# 2 Introduction

## 2.1 Scientific Backround

During the last few decades the modelling of catchment hydrology by spatially distributed models has been established as a tool for gaining insights to storage properties and runoff components (Wigmosta et al., 1994; Refsgaard, 1997; Wigmosta and Lettenmaier, 1999). Especially in mountaineous catchments with complex topography modeling approaches are needed that are able to capture the heterogeneity of the hydrolological system with respect to highly variable morphology, rainfall, snow melt and different types of soil and vegetation (Gurtz et al., 2003). Those models can be used to study changes in the hydrological cycle, which are suggested by climate change scenarios (e.g. OCCC, 2007) and therefore such knowledge is of great importance for the analysis of recent and future critical low-flow conditions and storage characteristics.

## 2.2 Objectives

The objectives of this thesis are the assessment of groundwater storage properties of the pre-alpine headwater catchment Rietholzbach and their influence on low-flow characteristics and resilience to hydrological drought. This is carried out by using the physically based hillslope model HillVi (Weiler and McDonnell, 2004) with parameters representing soil physical properties for modeling runoff and isotope transport.

# 3 Study Site

## 3.1 Geography

The Rietholzbach research catchment belongs to the Thur river basin which is a tributary of the Rhine. It is located in the pre-alpine zone of northeastern Switzerland with its center at approximately 47° 22' 54" northern latitude and 8° 59' 42" eastern longitude (Fig. 3.1).


**Figure 3.1:** Location of the Rietholzbach research catchment (modified map from the ETH Zurich website).

The Rietholzbach catchment covers an area of 3.18 $km^2$ belonging to the communities Kirchberg and Mosnang in Kanton St. Gall (Gurtz et al., 2006). According to grid data from the Institute for Atmospheric and Climate Science (ETH Zurich) used for the modeling in this thesis, its elevation ranges from 675 m to 935 m a.s.l. (Fig. 3.2). Various values for minimum and maximum elevation of the Rietholzbach catchment can be found in the literature. While according to Vitvar et al. (1999) and

König et al. (1994) elevations range from 680 m to 960 m a.s.l., Bohrer (1998) mentions 680 m to 949 m a.s.l. and Gurtz et al. (2006) speak of 682 m to 950 m a.s.l. The reason for these differences may be the use of digital elevation models with differing spatial resolutions or different methods of height specification.

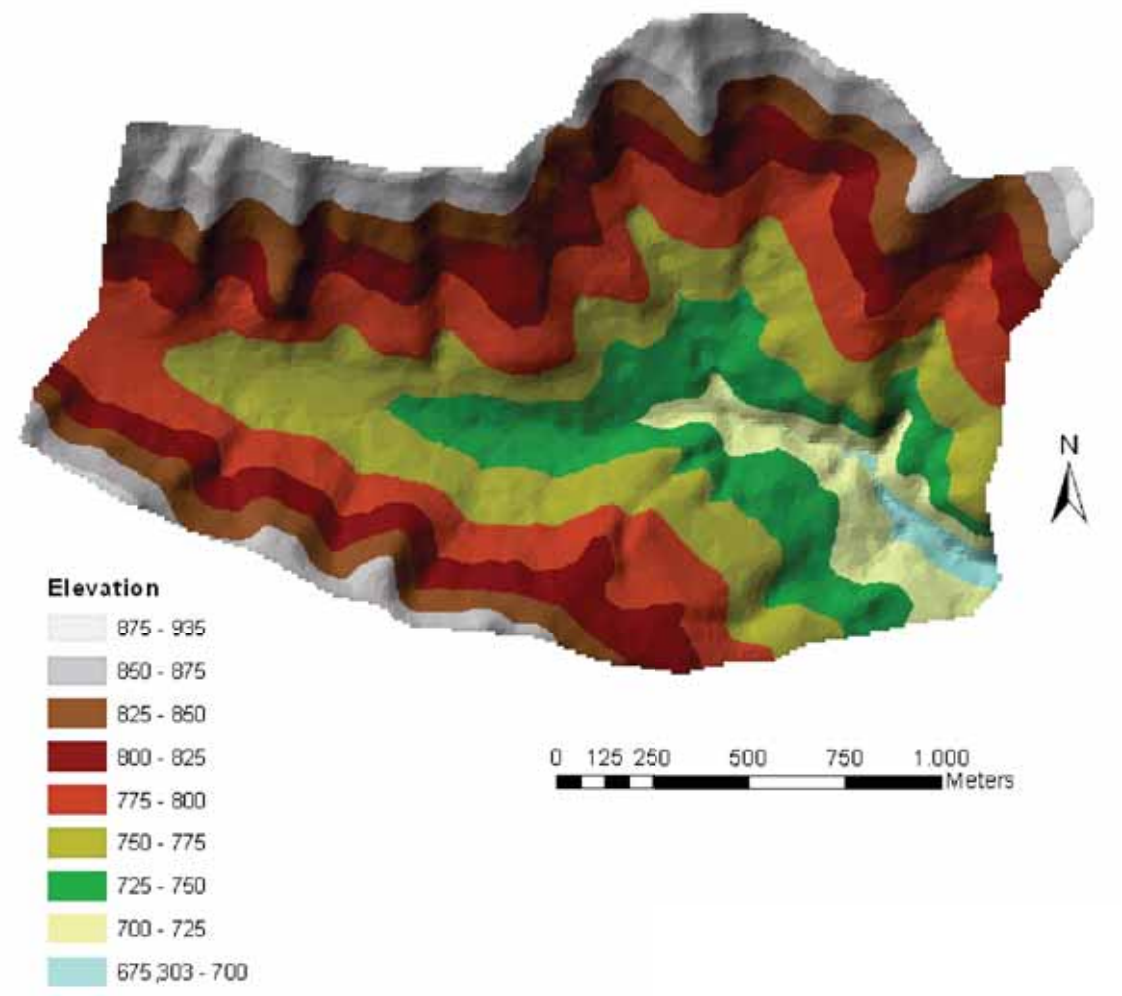


**Figure 3.2:** Visualization of the digital elevation model of the Rietholzbach catchment. Elevation given in meters.

The Rietholzbach creek, which has a length of 2.2 km, has its source in the western part of the site and drains it from west to east into the Gonzenbach. Accordingly the watershed's main valley is oriented west to east. Due to regressive erosion the Rietholzbach has deeply graved into the underlying sediments in its eastern part, creating some steep slopes in this region of the watershed and resulting in an unevenly longitudinal profile of the creek. Generally the Rietholzbach and its tributaries form a dendritic (Fig. 3.3) stream network (Gurtz et al., 2006). The valley's cross-section is assymetric (Gurtz et al., 2006) because the hillslopes exposed

to the north are steeper than those of the southface. The catchment's average slope accounts for 12.5° (Bohrer, 1998).

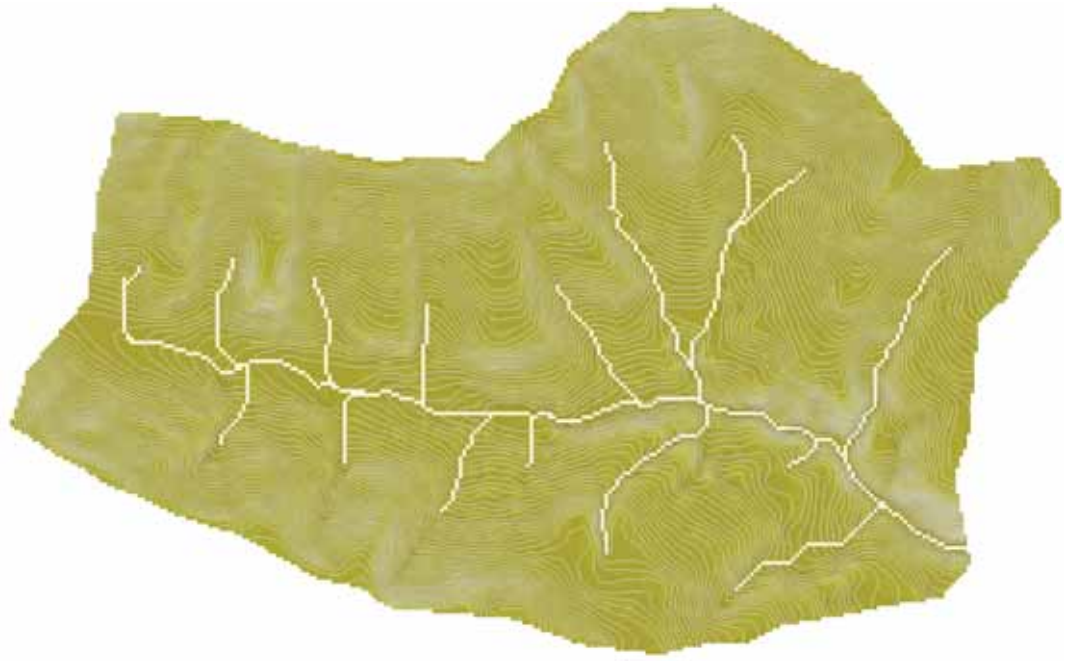

**Figure 3.3:** Stream network of the Rietholzbach catchment calculated with ArcGIS and based on a 10 m x 10 m digital elevation model. The result is in good agreement with Bohrer (1998).

## 3.2 Instrumentation

The instrumentation of the Rietholzbach research catchment is operated by the Institute for Atmospheric and Climate Science of the ETH Zurich. Since 1975 the meteorological and hydrological parameters of the Rietholzbach watershed have been measured with high temporal solution (Vitvar et al., 1999). A complete meteorological station is located in the center of the catchment at Büel together with a 2.2 m deep weighting lysimeter and 15 TDR probes continously measuring soil moisture at different depths up to 110 cm. Moreover there are three access tubes for groundwater level observations and three runoff gauging stations (Fig. 3.4).

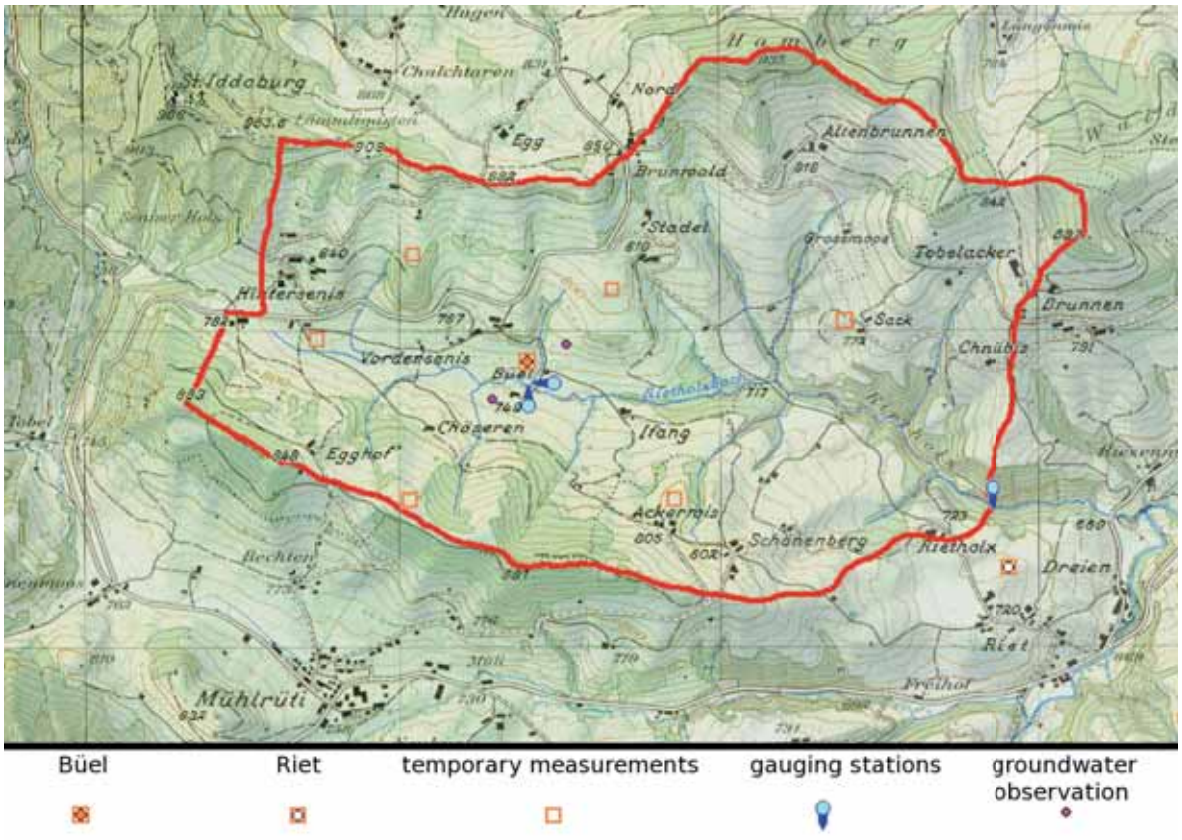


**Figure 3.4:** Measuring points of the Rietholzbach catchment (map modified from ETH Zurich).

The isotopic composition of the precipitation, the groundwater and the streamwater is continously detected on a semi-monthly basis. The regularly measured data is automatically transferred and some of the data is available online on a daily or even hourly basis (Gurtz et al., 2003).

## 3.3 Climate

Generally the Rietholzbach catchment has a montane to higher montane humid climate (Kuhn, 1980). Mean annual air temperatures at the station Büel account for slightly above 7 °C during the period 1976-2007. (Fig. 3.5). According to measurements at the station Büel beginning in 2000, an appreciable snow accumulation can be observed during winter, but the snow height rarely exceeds 0.5 m.

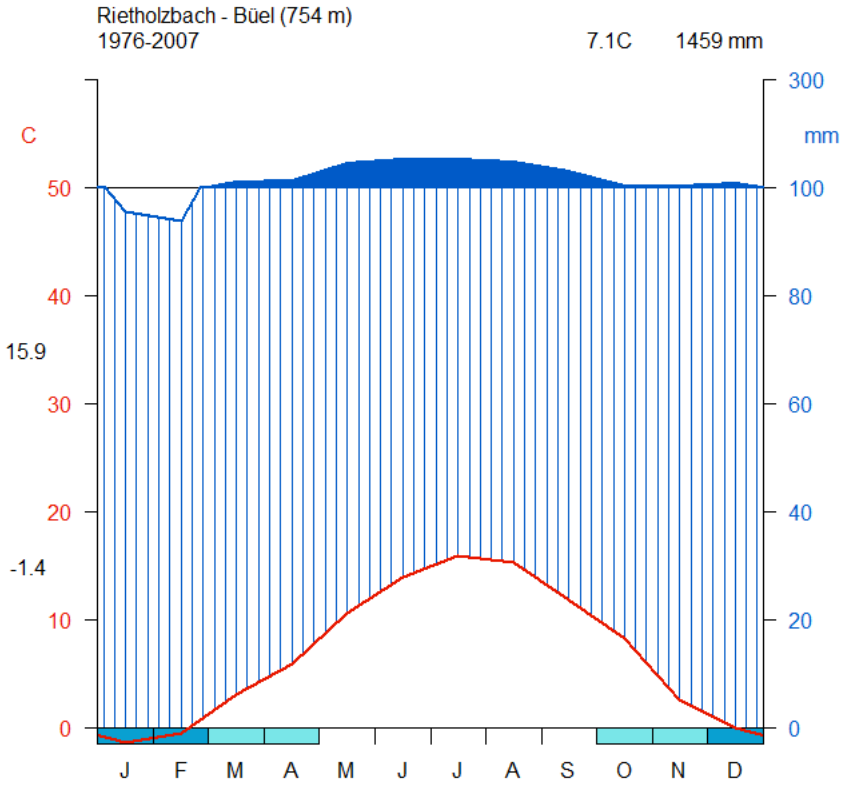


**Figure 3.5:** Climate diagram drawn according to Walter and Lieth (1960) of the meteorological station Büel based on the time period 1976-2007. The monthly average temperature of the warmest and of the coldest month is annotated in black at the left margin. The flat rectangles at the lower margin indicate whether the occurence of frost is sure (dark blue) or probable (light blue).

Since the beginning of temperature measurements in 1975 an unsteady trend of increasing temperatures can be observed, while precipitation patterns have remained the same (Gurtz et al., 2006).

The precipitation has a seasonal cycle typical of Switzerland's pre-alpine regions wita a maximum in summer. During the measurement period of 1976-2005 the annual sums of precipitation at the meteorological station Büel ranged from 1113.5 mm in 2003 to 1816 mm in 2001 with a mean value of 1450 mm (Gurtz et al., 2006). The data shows precipitation to occur very frequently, on an average of every three days during the aforementioned period. Droughts with several weeks of zero precipitation are exceptional phenomena in the Rietholzbach catchment.

**Table 3.1:** Average annual water balance of the Rietholzbach catchment. (König et al., 1994)

| | |
|---|---|
| Precipitation | 1600 mm |
| Runoff | 1040 mm |
| Evapotranspiration | 555 mm |

The average annual water balance (Tab. 3.1) shows that about two thirds of the precipiation contributes to runoff, which means the catchment generally has a high water availability. Usually the evapotranspiration is energy-limited, with the exception of longer dry periods like the summer drought of 2003 (Gurtz et al., 2006).

## 3.4 Soil and Land-use

Generally the literature distinguishes between 8 different soil types (Fig. 3.6) to be found in the Rietholzbach watershed (Kuhn, 1980; Germann, 1983).

According to Kuhn (1980) three different types of gleys with low permeabilities ($< 1 \times 10^{-8}\,\mathrm{ms^{-1}}$) are distributed along the Rietholzbach and its tributaries, covering about 63 % of the area (König et al., 1994). Especially in the higher regions of the catchment regosols and a variety of brown soils are abundant, all of them having a slightly higher saturated hydraulic conductivity of up to $5 \times 10^{-8}\,\mathrm{ms^{-1}}$. The mean saturated k-value of the soils for the whole catchment is estimated to be $1.8 \times 10^{-8}\,\mathrm{ms^{-1}}$ (König et al., 1994). According to Germann (1983) about 90 % of the area has a more or less well developed macropore system. Therefore, from a hydrological point of view and especially with respect to the generalizations that have to be made when modeling based on a grid with a side length of several meters, these low permeabilities are unlikely to be appropriate values to characterize saturated soil water movement throughout the watershed. The effective saturated hydraulic conductivity of the soils can be expected to be up to several orders of magnitude higher than the aforementioned saturated k-values.

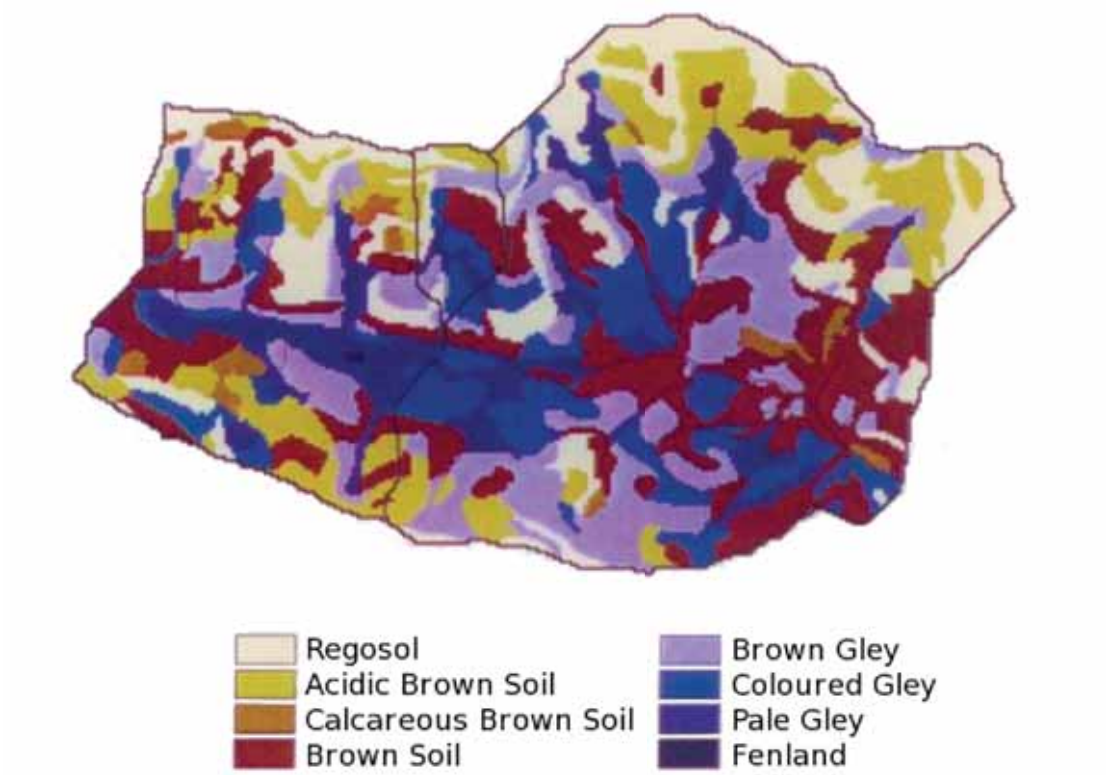


**Figure 3.6:** Distribution of soils in the Rietholzbach catchment according to Kuhn, 1980 (map modified from Bohrer, 1998).

Soil depths mostly range between 0.3 m and 1.0 m (Kuhn, 1980; Bohrer, 1998). About 60 % of the area consists of soils with a depth of more than 50 cm (König et al., 1994). Generally soil depths are higher (up to 2 m) in the catchment's lower regions near the bed of the valley and lowest (0.1 m - 0.3 m) at steep slopes (Kuhn, 1980; Bohrer, 1998).

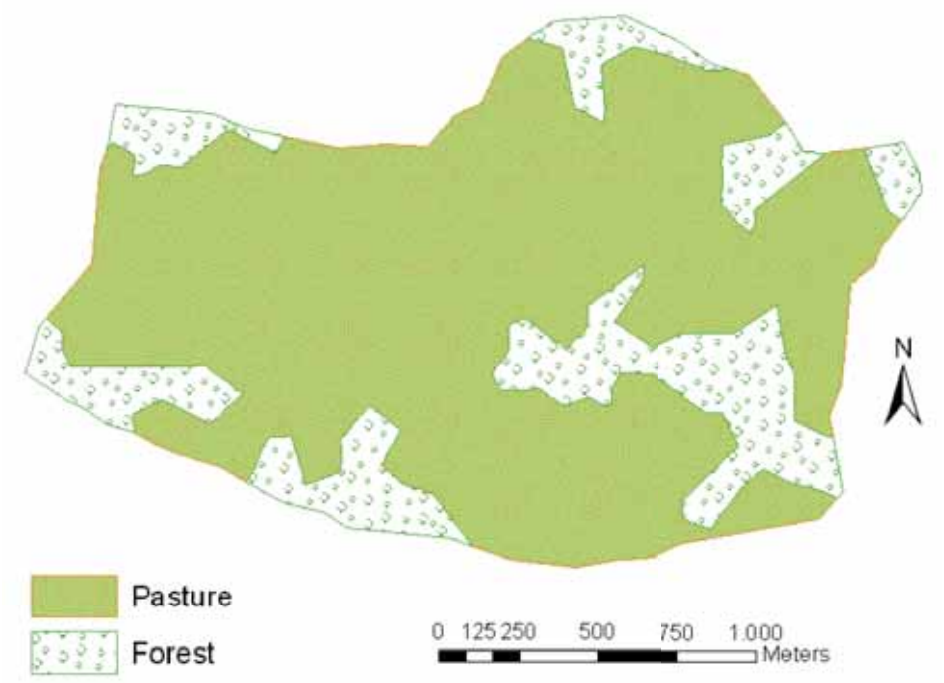


**Figure 3.7:** Land-use of the Rietholzbach catchment based on Corine Land Cover Mapping.

According to data from Corine Land Cover Mapping, which is based on satellite images, most of the Rietholzbach watershed is used as pasture land and only about 25 % are forested by mostly mixed forests (Fig. 3.7). Some of the pasture land in the higher regions of the catchment permanently has highly water saturated soils and therefore can be regarded as wet- or fenland (König, 1994; Vitvar, 1998). Photographs of the catchment originating from the mid 1970s show that land-use has not significantly changed since then. The area is sparsely populated with only a few farms and none of it can be regarded as settlement area (Bohrer, 1998). Conversations with local farmers and a Tracer Injection by Burgthaler in 1992 have brought to light that appreciable parts of the pasture land, especially in the higher regions of the catchment, are equipped with private drainage systems. There is no data available about their exact position and extent.

## 3.5 Hydrogeology

The geology of the Rietholzbach basin is typical for a swiss pre alpine headwater catchment, because it is dominated by clastic sedimentary deposits originating from the central parts of the alps (Fig. 4.6).

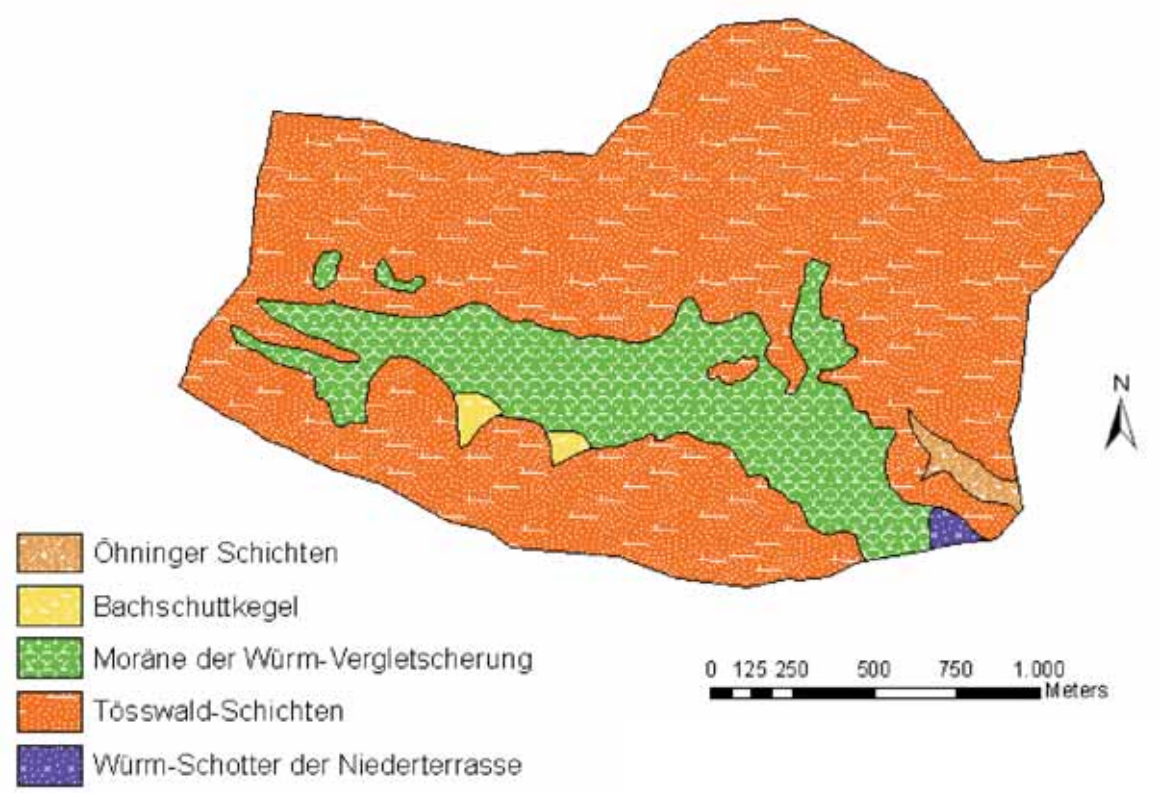


**Figure 3.8:** Geology of the Rietholzbach catchment.

Almost 80 % of the watershed are characterized by tertiary deposits of the Upper Freshwater Molasse, the "Tösswald-Schichten" and the "Öhninger-Schichten" (Bohrer, 1998). They consist of consolidated clastic sediments such as conglomerates (generally denoted as "Nagelfluh"), sandstones, layers of marls and banks of limestone. In the flat riparian zones along the Rietholzbach creek the "Tösswald-Schichten" are overlayed by sandy to silty Pleistocene gravel pockets originating from Würm glacier moraines (in Fig. 4.6: "Moräne der Würm-Vergletscherung" and "Würm-Schotter der Niederterasse"), which have a low clay-content (Vitvar et al., 1999; Gurtz et al., 2003). In the lower part of the basin's southface two stream debris cones can be found (in Fig. 4.6: "Bachschuttkegel").

The Upper Freshwater Molasse and the quarternary deposits in the valley bottom have a highly variable thickness of 2 m - 20 m (König, 1994) and serve as aquifers with medium to high hydraulic conductivities and relatively large storage capacities (Vitvar et al., 1999). Balderer (1982) generally decibes the Upper Freshwater Molasse as "a heterogenous system of interconnected aquifer layers". The mean depth of the stored water, which can be regarded as a mean thickness of the flow producing layer, has been calculated to be 7.1 m (Vitvar and Balderer, 1997). Measurements at the groundwater observation holes show groundwater levels to be highly variable

ranging between around 1 m and up to 6 m below ground level in the valley bottom at Büel. The entire water volume leaving the catchment can be measured at the gauging station Mosnang and the over- and underground watersheds are according (Gurtz et al., 2006).

Obtained by single well pumping tests carried out on groundwater boreholes (Vitvar, 1998) the hydraulic conductivitiy of the "Nagelfluh" amounts to $3.2 \times 10^{-5}$ ms$^{-1}$, while the saturated k-values of the quarternary deposits was detected to be about an order of magnitude higher accounting for $1.2 \times 10^{-4}$ ms$^{-1}$. These values are in good agreement with hydraulic conductivities derived by evaluations of discharge records from springs in the Aubach catchment which is located near the Rietholzbach basin and has the same geological properties (Balderer, 1982). Similar hydraulic conductivities for quarternary deposits can also be found in glacier moraines of southern Bavaria (Krause, 2000). The mean porosity of the catchment's groundwater storage is estimated to be 7.5 % (Vitvar and Balderer, 1997).

## 3.6 Runoff

The Rietholzbach creek has a variable hydrological regime with very fast and strong responses to rainfall events (Fig. 3.9).

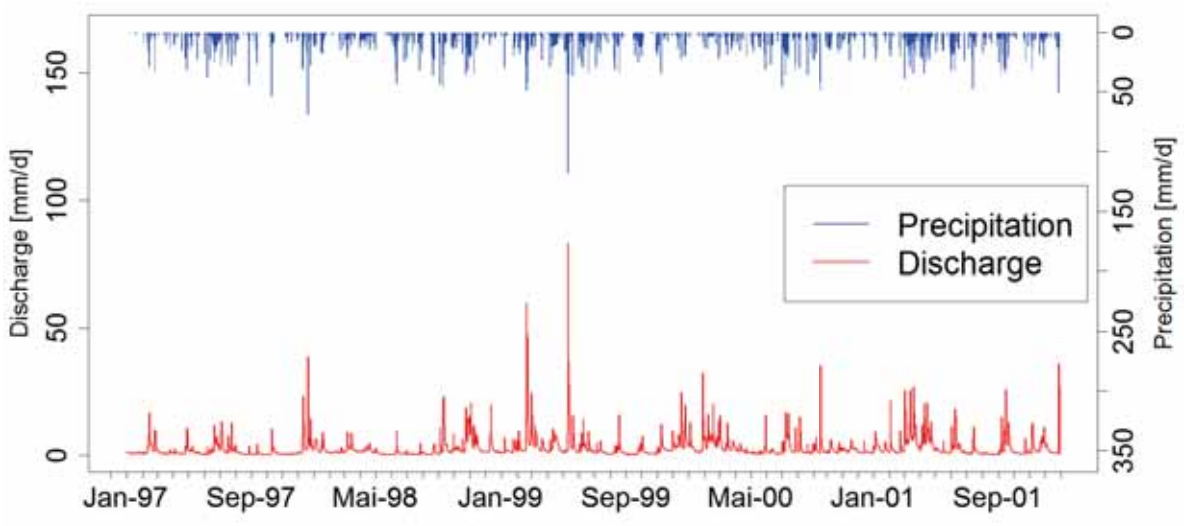


**Figure 3.9:** Discharge at the gauging station Mosnang and Precipitation at the meteorological station Büel (measured 0 m above ground level) during the time period 1997 - 2001.

A comparison of the amount of mean discharge MQ (Tab. 3.2) at the gauging station Mosnang and the corresponding flow duration curve (Fig. 3.10) show the distribution of outflows over time to be strongly skewed. Most of the time the Riet-

holzbach creek has a discharge far below its mean value MQ, the most frequent value Mode Q is even lower than the calculated Q90 (Fig. 3.10).

**Table 3.2:** Hydrographic characteristics of the Rietholzbach creek, derived from mean daily values of the years 1975 - 2008.

| | | |
|---|---|---|
| NQ | (lowest mean daily value of the observation period 1975 - 2008) | 1.9 l/s |
| MNQ | (average of each year's lowest mean daily value during 1975 - 2008) | 8.1 l/s |
| MQ | (average of all mean daily values of the observation period 1975 - 2008) | 105.8 l/s |
| MHQ | (average of each year's highest mean daily value during 1975 - 2008) | 1335.0 l/s |
| HQ | (highest mean daily value of the observation period 1975 - 2008) | 2923.3 l/s |
| Median Q | | 53.1 l/s |
| Mode Q | | 11.95 l/s |

There is a moderate seasonal variation in the mean monthly discharge (Fig. 3.11) with highest values associated to snow melt in spring and lowest in July and August.

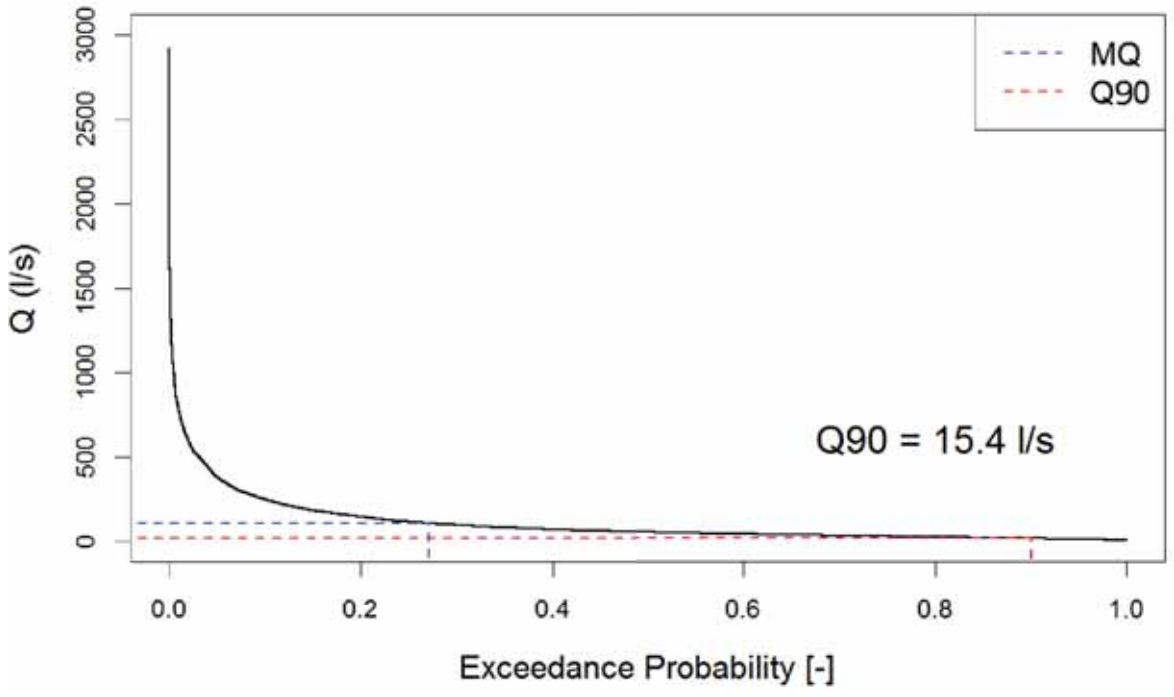


**Figure 3.10:** Flow duration curve of the Rietholzbach creek based on mean daily values of 1975-2008.

Since the beginning of continous discharge measurements in 1975, the Rietholzbach creek has never dried out completely. If Q90 as a constant threshold for the

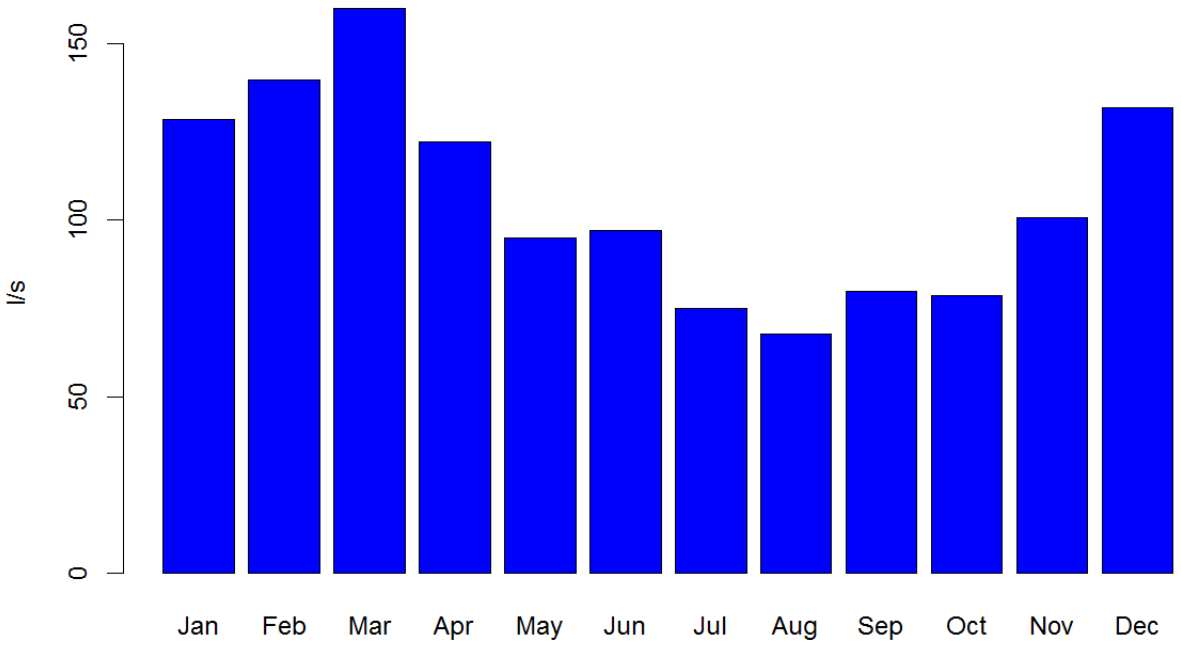


**Figure 3.11:** Mean monthly discharge calculated from mean daily values of 1975 - 2008.

defintion of low-flow conditions is chosen (Hisdal and Tallaksen, 2000) and compared with the temporal variation of discharge (Fig. 3.9 & Fig. 3.11), it becomes obvious that low-flows occur frequently but seldom last longer than a few days.

# 4 Methodology

## 4.1 HillVi - Model Concept

HillVi is a physically based hillslope model written in IDL[1]. It has been used as tool for the identification of main flow processes and simulation of mass transport in hillslopes (Weiler et al., 2003; Weiler and McDonnell, 2004, 2006, 2007; Gascuel-Odoux et al., 2010). HillVi is based on a grid cell by grid cell approach that allows for a spatially explicit conceptualisation of the water balance within the saturated and unsaturated zone with respect to soil physical properties (Weiler and McDonnell, 2004). Each grid cell is based on an elevation point of a digital elevation model (DEM) with corresponding soil depth information and consists of an unsaturated and a saturated zone (Weiler and McDonnell, 2006). The saturated zone is defined by the height of the water table, which is recalculated with every time step, while the unsaturated zone is defined by its temporaly variable water content (Weiler and McDonnell, 2007). The explicit representation of the saturated and unsaturated zones and the tight coupling between the two storages has been implemented because hillslope studies have shown that a perched water table within the soil, converting unsaturated to saturated zone, is the most common process for delivering water downslope towards the valley bottom (McGlynn et al., 2002; Weiler and McDonnell, 2004).

The different storages and flow mechanisms implemented in HillVi are represented schematically in Fig. 4.1. Water input into the system is only provided by precipitation, either directly as rain or indirectly as snowmelt. There is no lateral subsurface inflow to the model domain. Output in the form of discharge is generated by the amount of saturated subsurface flow (SSF) which is routed into cells defined as channel cells. All water entering a channel cell is immediately removed from the system. If a grid cell is completely saturated, all water volume exceeding its total storage capacity is immediately removed from the domain and accounts for discharge as well. The water volume due to evapotranspiration which is calculated with respect to available soil moisture, is removed from the unsaturated storage straight

[1] in this thesis IDL Student Edition 6.2 by Research Systems Inc. was used

away. In case this water volume exceeds the unsaturated storage or in the case of complete saturation of a cell removal occurs from the saturated storage.

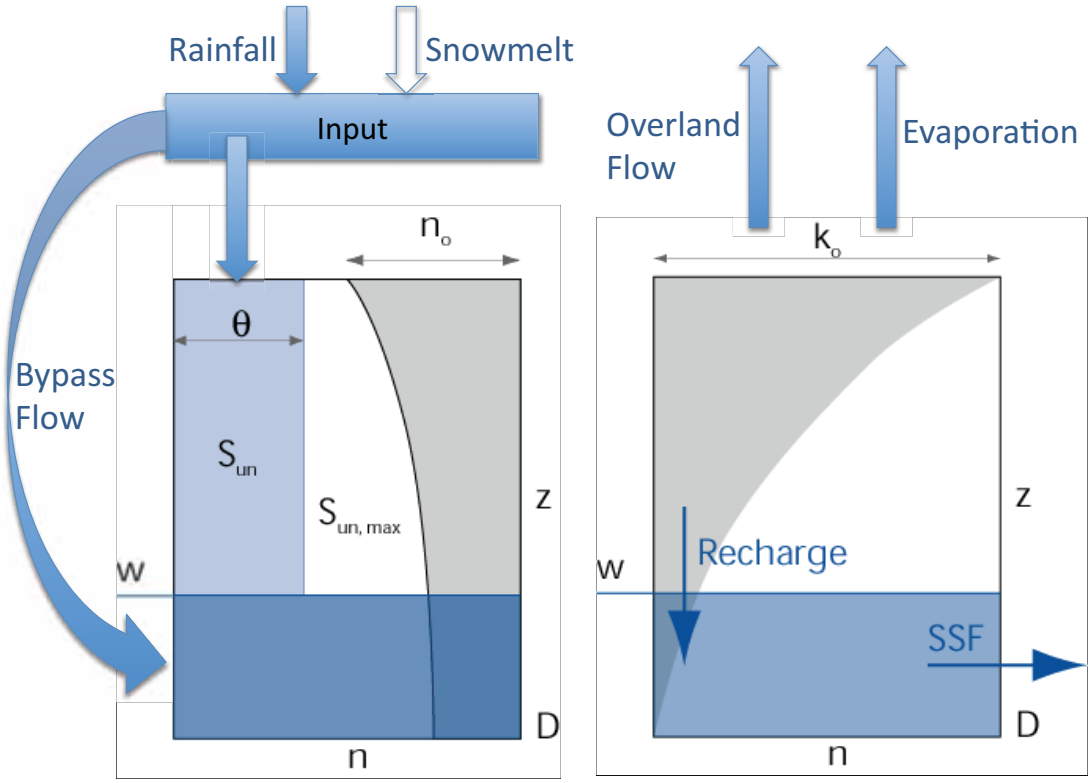


**Figure 4.1:** Schematic of storages, depth distributions of drainable porosity and saturated hydraulic conductivity and flow mechanisms used in HillVi. $S_{un}$ is the unsaturated storage, $S_{un,max}$ is the maximum unsaturated storage, θ is the actual water content of the unsaturated storage, n is the total porosity, $n_0$ is the drainable porosity at the soil surface, $k_0$ is the saturated hydraulic conductivity at the soil surface, z is the depth to the watertable, D is the total soil depth and w marks the position of the watertable (schematic modified from Weiler et al., 2003).

The saturated subsurface flow is calculated according to the explicit grid cell by grid cell approach described by Wigmosta et al. (1994). This approach has been evaluated using a series of numerical experiments and was found to be in good agreement with analytical solutions in all test cases (Wigmosta and Lettenmaier, 1999). It is based on the Dupuit-Forchheimer assumption, which is an easily understandable but sufficient representation of the aforementioned physical process of perched water table development and the resulting lateral water movement (Freeze and Cherry, 1979). The practical application is described in Wigmosta and Lettenmaier (1999) as follows: Each grid cell is centered at an elevation point of the DEM and is able to exchange water with its eight surrounding grid cells (Fig. 4.2). As illustrated

in Fig. 4.2 all adjacent cells are numbered from 0-7. The local gradient between the centered cell and its neighbours is then calculated by local water table slopes. Utilizing the indices drawn in fig. 4.2 and adding an index k for each possible direction, the rate of saturated subsurface flow can subsequently be calculated via

$$q_{i,j,k} = \begin{cases} T_{i,j,k} \quad G_{i,j,k} \quad w_{i,j,k} & G_{i,j,k} > 0 \\ 0 & G_{i,j,k} \leqq 0 \end{cases} \tag{4.1}$$

where $q_{i,j,k}$ is the flow rate from cell i,j in k direction, $T_{i,j,k}$ is the transmissivity at cell i,j corresponding to the k direction, $G_{i,j,k}$ is the water table gradient from cell i,j towards its neighbouring cell in k direction and $w_{i,j,k}$ is the width of flow (Wigmosta and Lettenmaier, 1999; Hirzel, 2009). In the light of this formula it becomes obvious that, in contrast to many other models, HillVi recalculates the outflow from each grid cell for each time step based on the local water table gradient. For this reason HillVi is able to simulate hillslopes with a spatially variable soil depth and local depressions in the bedrock surface without constraining the outflow in the corresponding grid cells to zero (Weiler and McDonnell, 2004).

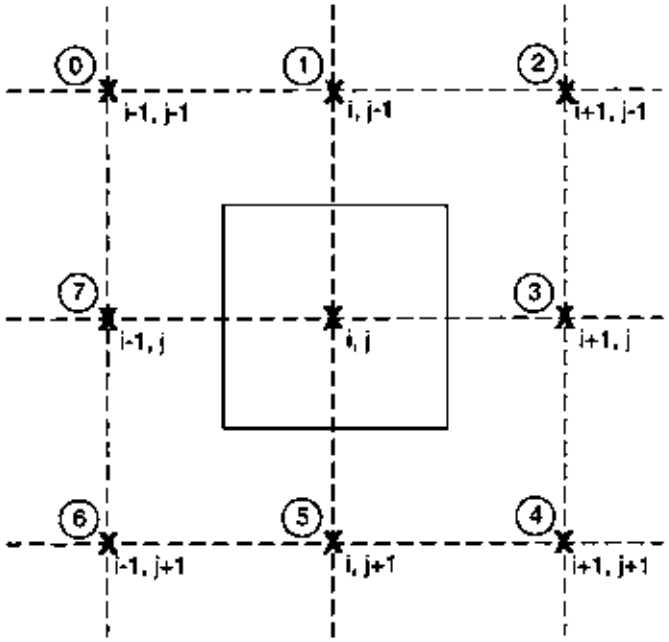


**Figure 4.2:** Computational scheme of the grid cell to grid cell approach (schematic from Wigmosta and Lettenmaier, 1999).

In order to represent the increasing compaction of the soil with depth, the transmissivity is calculated with respect to an exponential decline of the saturated hydraulic conductivity with depth by the expression

$$T(z) = \int_{z(t)}^{d} K_s(z)dz = K_0 m \cdot \left[ e^{\frac{-z}{m}} - e^{\frac{-d}{m}} \right] \tag{4.2}$$

where T represents the transmissivity depending on the depth of the flow, $K_s$ the saturated hydraulic conductivity, $K_0$ the saturated hydraulic conductivity at the soil surface, m the shape parameter of the exponential function, z the depth into the soil profile (positive downwards) and d the total soil depth (Weiler et al., 2003).

Because of the major influence of the soil's retention characteristics on saturated subsurface flow in the absence of macropores and for the transient water table development (Weiler and McDonnell, 2004) a function for drainable porosity is implemented in HillVi. The drainable porosity is the difference in volumetric water content between saturated water content and soil water content at a water tension of 100 cm, which approximately corresponds to field capacity (Weiler and McDonnell, 2006, 2007). It usually declines with depth according to the saturated hydraulic conductivity and therefore is expressed with a depth function similar to those of $K_s$, formulated as follows:

$$n_d(z) = n_0 \cdot e^{\frac{-z}{b}} \tag{4.3}$$

where $n_d$ is the drainable porosity at depth z, $n_0$ is the drainable porosity at the soil surface, z is the depth into the soil profile and b is a decay parameter (Weiler and McDonnell, 2004).

As the precipitation input is not directly routed to the saturated zone but to the unsaturated zone, a recharge function that describes a nonlinear response to increasing soil water content is required. There have been several approaches to the recharge function in HillVi. The expression taken as basis for this thesis takes into account the relative water content of the unsaturated zone and the local hydraulic conductivity. It is described in McGuire et al. (2007) and is given by

$$R(t) = \left( \frac{\theta(t)}{\theta_s} \right)^c K_0 \cdot e^{\left(\frac{-z}{m}\right)} \tag{4.4}$$

where R is recharge to the saturated zone, $\vartheta/\vartheta_s$ is the relative water content of the unsaturated zone, c is the power coefficient to force a nonlinear response to increasing soil moisture content, $K_0$ is saturated hydraulic conductivity at the soil surface, z is the depth of the water table surface under the ground (positive downwards) and m is the hydraulic conductivity shape factor mentioned earlier. See *Appendix 2* for the IDL-code of the recharge flow routine.

Furthermore, a bypass term has been introduced to HillVi that allows for a wet-

ness dependant direct recharge of precipitation into the saturated zone. Bypass flow is an often observed process in hillslope studies (McDonnell, 1990; Leaney et al., 1993; Buttle and McDonald, 2002). Slightly modified from McGuire et al. (2007) by using infiltration instead of precipitation as a coefficient it is expressed by

$$q_{bp}(t) = I_{in} \left( \frac{\theta(t)}{\theta_s} \right)^{\beta} \tag{4.5}$$

with $q_{bp}$ as bypass flow, coefficient $I_{in}$ as infiltration rate, $\vartheta/\vartheta_s$ as relative water content and $\beta$ as bypass power exponent. See *Appendix 3* for the code of the bypass flow function.

The actual evaporation rate is as well calculated as fraction of the relative water content of the unsaturated zone and is given by

$$E_{act}(t) = E_{pot} \left( \frac{\theta(t)}{\theta_s} \right) \tag{4.6}$$

where $E_{act}$ is the actual evaporation rate and $E_{pot}$ is the potential evaporation rate. The code for the evaporation routine is given in *Appendix 4*.

Snow accumulation and snow melt procedures are also implemented in HillVi under consideration of air temperature, precipitation, present snow pack, retained liquid water and refreezing. See *Appendix 5* for the code of the snow routine.

The water balance of the unsaturated zone is determined by the precipitation input, the vertical recharge into the saturated zone, the evapotranspirational loss and its resulting change in water content. The water balance of the saturated zone is calculated by the recharge input, the direct vertical input from bypass flow, the lateral inflow and outflow to the surrounding grid cells due to water table gradients and the corresponding change in water table depth. The IDL code for the calculation of the water balance in the saturated and the unsaturated zone can be found in *Appendix 6*.

## 4.2 Model Modifications

HillVi was originally intended as a hillslope model without accounting explicitly for streams, but the implementation of channel cells can easily be performed by creating a grid of the same size as the DEM of the catchment topography which assigns a value of 1 to each cell appointed as a channel cell. The channel cells shown in Fig. 4.3 were defined with ArcGIS by calculating flow directions and flow acccumulation based on the $25\,\mathrm{m} \times 25\,\mathrm{m}$ grid that was used for the modeling.

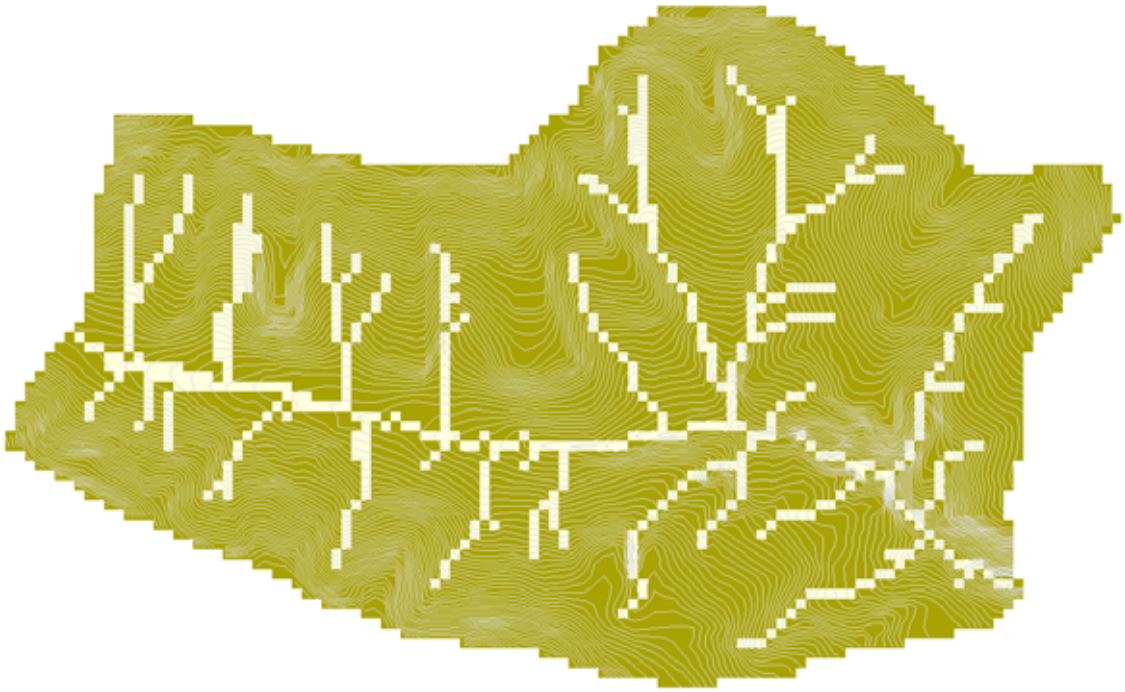

**Figure 4.3:** Calculated stream network based on 25x25 m DEM of the Rietholzbach catchment

The reason for implementing channel cells is that model test runs with an outlet defined at the lowest point of the catchment but not accounting for streams showed an incorrect representation of the flow mechanisms leading to discharge. In this case runoff was mostly created by exceeding cell storages.

To gain insights into transit times and to be able to improve model calibration by using observed isotopic composition in discharge as an additional criteria, an isotope transport routine was implemented in HillVi. It is based on complete mixing assumptions in both the unsaturated and saturated storage. The isotopic composition of both storages for every timestep is therefore controlled by the isotopic compositions and water volumes of the several inflows at the present timestep, the corresponding change in water table height and the original isotopic compositions of the storages themselves. The isotope transport routine is schematically represented in Fig. 4.4. The isotopic composition of the unsaturated storage is calculated under consideration of $\delta\ ^{18}O$ of the infiltration, the water volume that is retained in the soil when the watertable is falling and the unsaturated storage volume of the previous timestep. For the calculation of the isotopic composition of the saturated storage the $\delta\ ^{18}O$ from recharge, bypass flow, saturated subsurface flow, the water volume of the unsaturated storage which is included into the saturated storage when the watertable is rising and the saturated storage one timestep before is taken into account.

For the code of the isotope transport routine see *Appendix 7*.

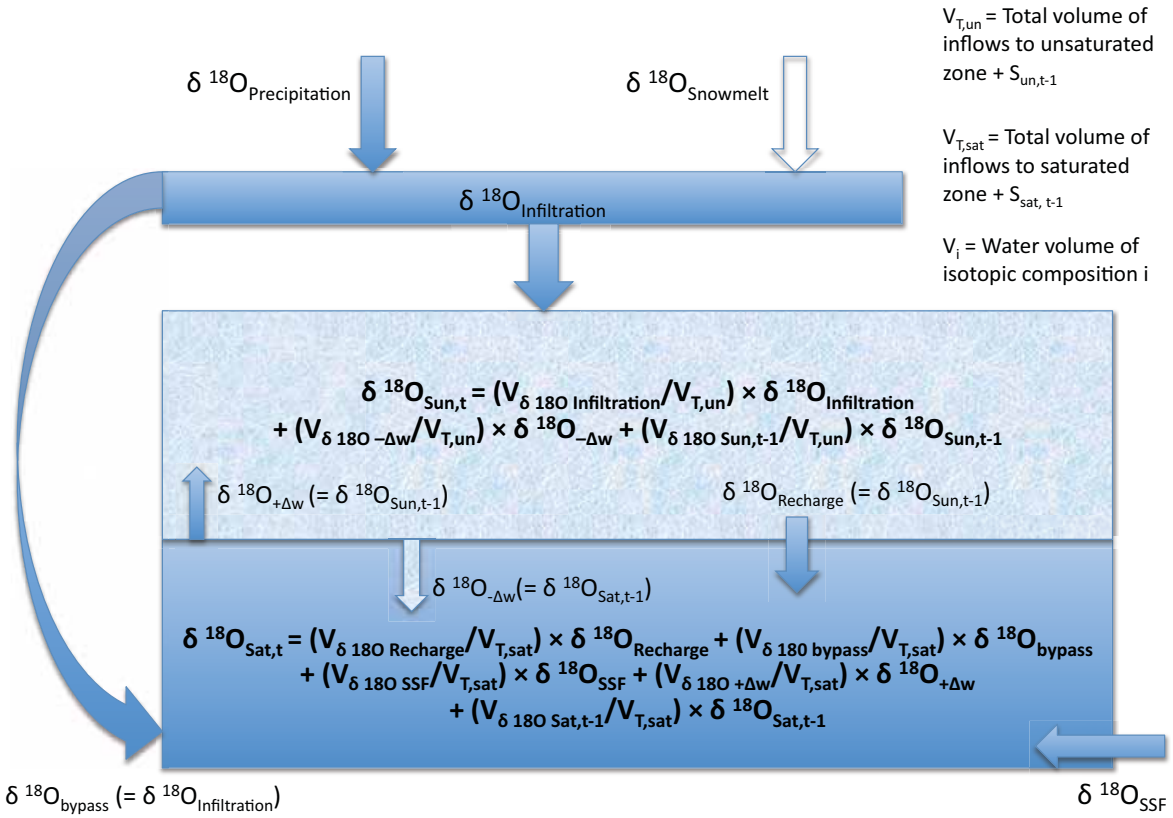


**Figure 4.4:** Schematic of the isotope transport routine. $S_{un,t}$ is the water content of the unsaturated storage at the current timestep, $S_{sat,t}$ is the water content of the saturated storage at the current timestep.

As illustrated in Fig. 4.4 the $\delta\ ^{18}O$ of the infiltration is determined with respect to input from snowmelt. The isotopic composition of the snowpack the liquid water is originating from is calculated as the mean isotopic composition of the precipitation input since the beginning of the current snow accumulation. In *Appendix 8* the respective code is given. The isotope transport routine neglects the influence of evaporation on the isotopic compositions of the storages because there are no isotopic fractionation processes implemented.

Because HillVi is primarily designed for water flow processes only in soil, some modifications were required to incorporate a spatially variable soil depth together with a representation of the underlying geological layer. The soil was defined as a top layer with high saturated hydraulic conductivity due to macropores and a rapid exponential decline of the latter with depth. The shape parameter m controls the degree of exponential decline as can be easily seen in the following formula

$$K_s(z) = K_0 \cdot e^{\frac{-z}{m}} \tag{4.7}$$

with $K_s$ as saturated hydraulic conductivity, $K_0$ as saturated hydraulic conductivity at the soil surface, z as the depth of the water table surface under the ground (positive downwards) and m as hydraulic conductivity shape factor. Using this formula two extreme values for m were caculated which represent the maximum and minimum thickness of the soil layer occuring throughout the catchment. According to Kuhn (1980) and Bohrer (1998) the soil depth ranges from several centimeters at steep slopes up to 2 m in the valley bottom. Therefore, when defining the hydraulic conductivity at the bottom of the soil layer to be 0.1 of its highest value, the highest and lowest value of m are calculated as follows:

$$m_{max} = \frac{-z}{\ln(0.1)} = \frac{-2m}{-2.303} = 0.8686m \tag{4.8}$$

$$m_{min} = \frac{-z}{\ln(0.1)} = \frac{-0.25m}{-2.303} = 0.1086m \tag{4.9}$$

Under the assumption that soil depths are primarily controlled by the topography, the spatial distribution of the shape parameter is then calculated as the linear function of the slope. Slopes were determined for each cell of the DEM resulting in a maximum slope of 40° and a minimum slope of 0° (Fig. 4.5). By assigning $m_{max}$ to a slope of 0° and $m_{min}$ to a slope of 40° the following linear function is derived:

$$m_i = -0.019 \cdot slope_i + 0.8686 \tag{4.10}$$

Where $slope_i$ is the slope of the corresponding grid cell, while $m_i$ is the value of m assigned to the grid cell i.

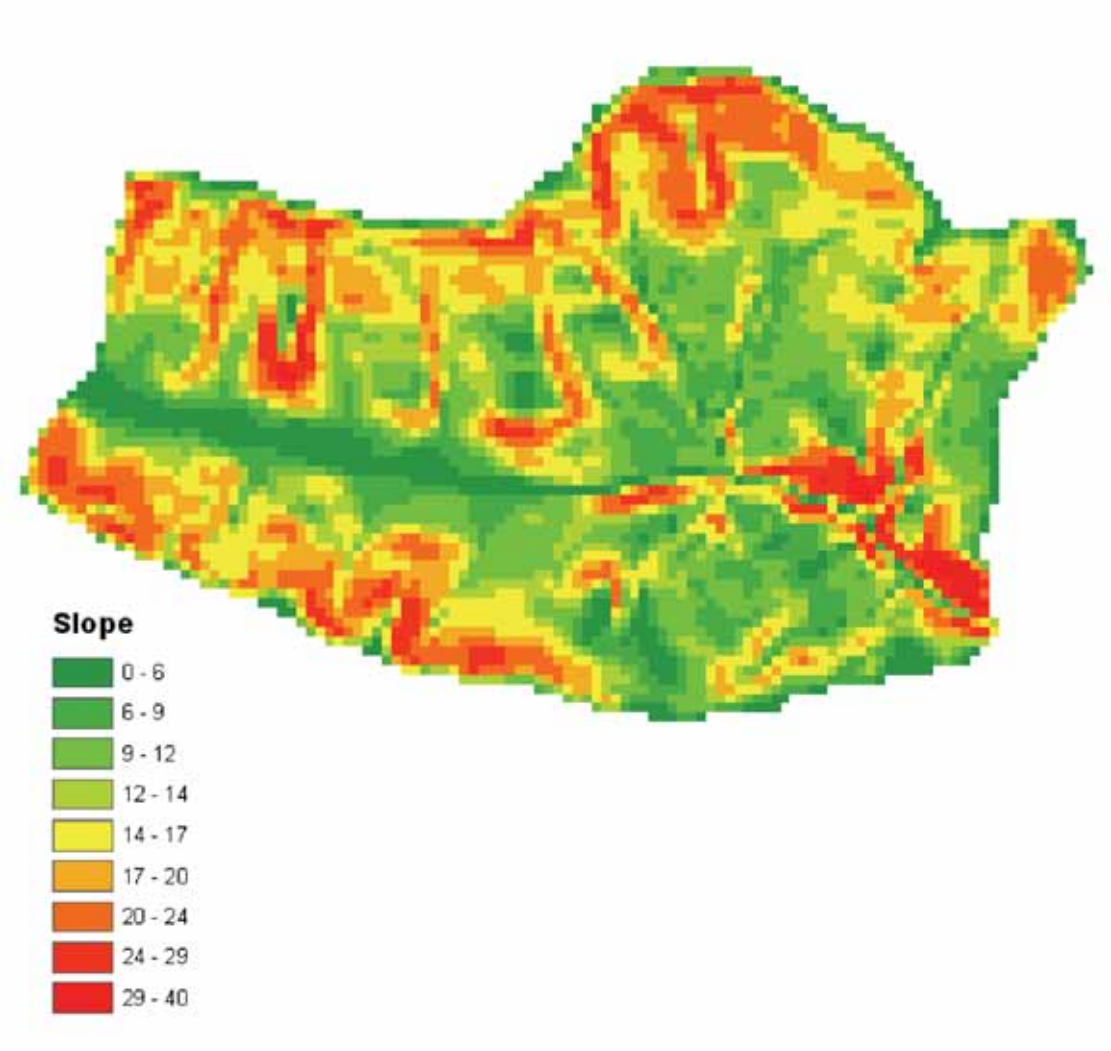


**Figure 4.5:** Slopes in degrees calculated on the basis of a 25x25 m DEM of the Rietholzbach basin

Besides the soil depth, a spatially explicit representation of the geology was implemented similar to Haas (2009), Hirzel (2009) and Gascuel-Odoux et al. (2010) by adding a constant to the formula that describes the exponential decline with depth of the saturated hydraulic conductivity:

$$K_s(z) = K_0 \cdot e^{\frac{-z}{m}} + K_{c,geo} \tag{4.11}$$

$K_{c,geo}$ being the saturated hydraulic conductivity of the respective geological unit is assigned to each grid cell according to its position in the catchment. Two different geological units were defined, the Nagelfluh located at the slopes of the Rietholzbach basin and the quarternary deposits forming the valley sediments (Fig. 4.6).

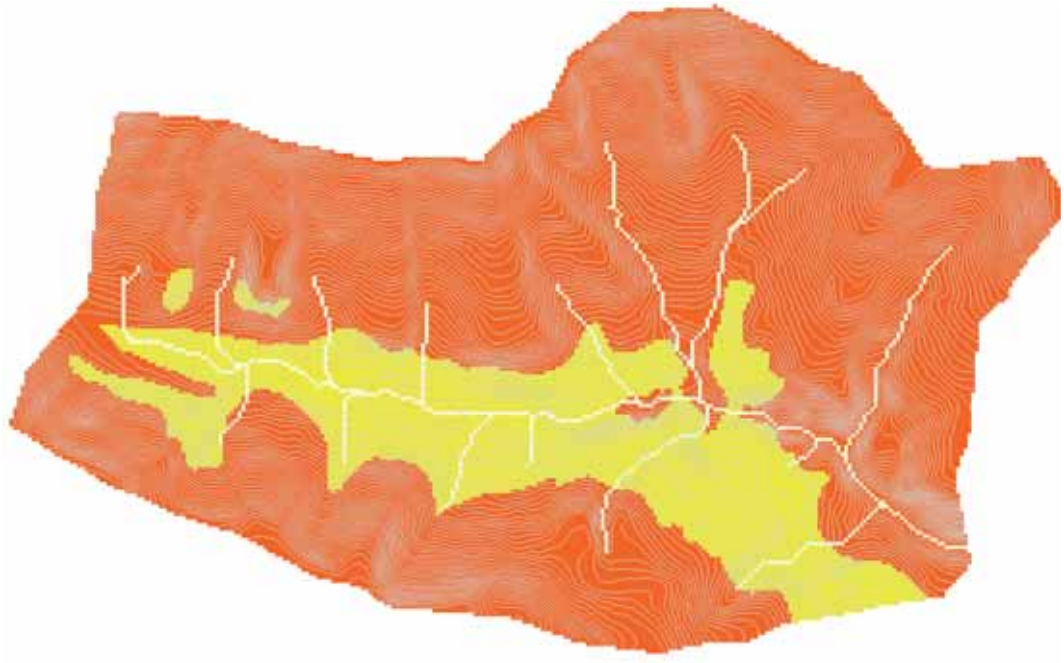

**Figure 4.6:** The position of the geological units that were distinguished for the modeling. Nagelfluh is coloured red, the quarternary deposits yellow.

Because it renders significant improvements of simulation time, the array based approach of saturated subsurface flow routing with implementation of $K_{c,geo}$ introduced by Hirzel (2009) was used.

## 4.3 Input Data and Model Setup

The modeling is based on hourly climate and runoff data and on semi-monthly isotopic data recorded from 01.01.1997 - 31.12.2001.

Data of temperature, wind speed, global radiation and relative humidity of the air, all recorded at Büel climate station, were used for the calculation of potential evaporation. The calculation of daily potential evaporation was performed by using Penman's approach for grassland (Penman, 1948) which considers both the influence of aerodynamics (right term in the numerator) and the radiation balance (left term in the numerator) and is calculated by

$$E_{pot} = \frac{\Delta \cdot EH + \gamma \cdot f(v) \cdot (e_s - e_a)}{\Delta + \gamma} \tag{4.12}$$

Here, $E_{pot}$ is the potential Evaporation, $\Delta$ is the gradient of the saturated vapour pressure curve, EH is the net radiation equivalent, $\gamma$ is the psychrometer constant, f(v) is the wind function, $e_s$ is the saturated vapour pressure and $e_a$ is the vapour

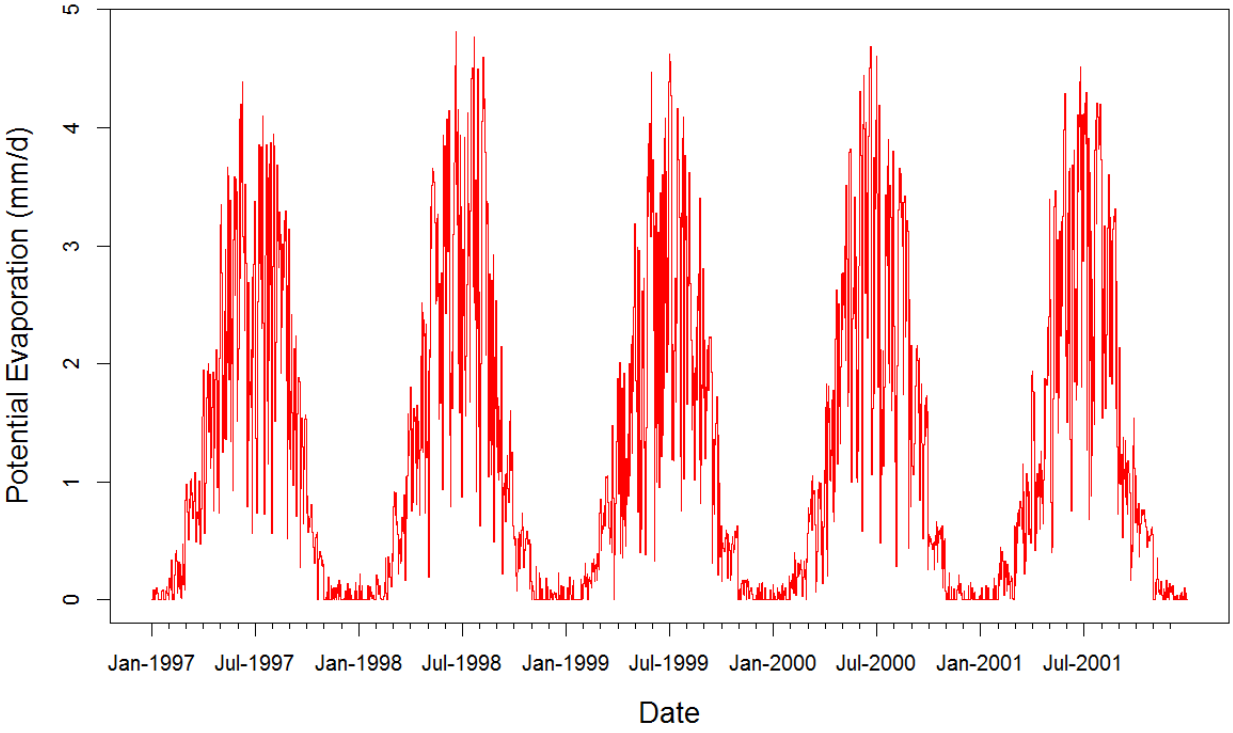


**Figure 4.7:** Daily values of calculated potential evaporation

pressure. The complete calculation procedure can be found in *Appendix 1*. The calculated $E_{pot}$ shows an obvious seasonal variation (Fig. 4.7) and amounts to an average of 458 mm per year during the period 01.01.1997 - 31.12.2001.

The model runs were performed with a one-hour timestep and used the following input data, all measured at Büel climate station: Precipitation measured at ground level, air temperature measured at 2 m above ground level, calculated potential evaporation and isotopic data of the precipitation. The model was calibrated by runoff and isotopic data of the streamflow both recorded at the gauging station Mosnang. To keep the duration of the model runs within reasonable limits a 25 m $\times$ 25 m grid has been used for the Monte Carlo simulations, although a more highly resolved grid of 10 m $\times$ 10 m has been available.

Early model test runs showed that there is a significant underestimation of modeled actual evaporation compared to literature values. It only accounted for about two thirds of the potential evaporation. In an energy limited system with high water availability the actual evaporation should be exspected to be close to the potential evaporation. For the Rietholzbach catchment this view is supported by lysimeter data. Therefore Monte Carlo simulations with forcing $E_{act} = E_{pot}$ were also well per-

formed, to test if this improves model efficiency and plausibility.

All data used for modeling has been provided by the Institute for Atmospheric and Climate Science (ETH Zurich).

## 4.4 Objective Functions

As objective functions for assessing the model quality concerning discharge the Nash-Sutcliffe efficiency (NSE) introduced by Nash and Sutcliffe (1970) was used that is calculated as:

$$NSE = 1 - \frac{\sum_{i=1}^{n} \left(Q_{obs}(i) - Q_{sim}(i)\right)^2}{\sum_{i=1}^{n} \left(Q_{obs}(i) - \overline{Q}_{obs}\right)^2} \tag{4.13}$$

with $Q_{obs}$ (i) as observed streamflow for timestep i, $Q_{sim}$(i) as the simulated streamflow for timestep i and $\overline{Q}_{obs}$ as the mean value of all observed streamflows. In order to obtain a better insight to the model quality with respect to low-flow, the NSE has also been calculated for a logarithmically transformed time series of $Q_{obs}$ and $Q_{sim}$ with:

$$\ln(NSE) = 1 - \frac{\sum_{i=1}^{n} \left(\ln(Q_{obs}(i)) - \ln(Q_{sim}(i))\right)^2}{\sum_{i=1}^{n} \left(\ln(Q_{obs}(i)) - \ln(\overline{Q}_{obs})\right)^2} \tag{4.14}$$

The efficiency of the isotope transport routine was evaluated by calculating the root mean square error (RMSE) of measured $\delta^{18}$O in relation to modeled $\delta^{18}$O of the discharge. The corresponding formula is given as:

$$RMSE_{\delta^{18}O} = \sqrt{\frac{\sum_{i=1}^{n} (\delta^{18}O_{obs}(i) - \delta^{18}O_{sim}(i))^2}{n}} \tag{4.15}$$

with $\delta^{18}O_{obs}$ (i) as observed isotopic composition in the streamflow for timestep i and $\delta^{18}O_{sim}$(i) as the simulated isotopic composition in the streamflow for timestep i.

## 4.5 Calibration, Validation and Uncertainty Analysis

A large number of test runs were performed to obtain appropriate parameter ranges containing good likelihood measures with respect to NSE, ln(NSE) and $RMSE_{\delta^{18}O}$.

Afterwards a final Monte Carlo simulation for each model configuration concerning evaporation (see section 4.3) was carried out. The final Monte Carlo simulation with the $E_{act} = E_{pot}$ configuration consisted of 1500 test runs, while those with the modeled $E_{act}$ consisted of just 900 test runs because of an error in writing the required output files. The model parameters and the parameter ranges have been the same for both configurations and are described in Tab. 4.1.

**Table 4.1:** Description and range of parameters used for Monte Carlo simulations

| name | description | min. | max. | range obtained from |
|---|---|---|---|---|
| n | total porosity | 0.07 [-] | 0.08 [-] | (König, 1994; Vitvar and Balderer, 1997) |
| n0 | drainable porosity at soil surface | 0.025 [-] | 0.035 [-] | model test runs |
| b | shape parameter of exponential depth function of drainable porosity | 2.5 [m] | 4.5 [m] | model test runs |
| k0 | saturated k-value at soil surface | 0.8 [m/h] | 1.2 [m/h] | model test runs, consideration of macropores and drainages |
| kc_n | saturated k-value of “Nagelfluh” | 0.15 [m/h] | 0.36 [m/h] | model test runs, (Balderer, 1982; Vitvar, 1998) |
| kc_q | saturated k-value of quarternary deposits | 0.15 [m/h] | 0.36 [m/h] | model test runs, (Balderer, 1982; Vitvar, 1998; Krause, 2000) |
| c | exponent of recharge function | 10 [-] | 30 [-] | model test runs |
| byp | exponent of bypass function | 1.5 [-] | 2.5 [-] | model test runs |
| d | total thickness of simulated layer | 9 [m] | 10 [m] | model test runs, 7.1 m mentioned inVitvar and Balderer (1997) + considering unsaturated layer |

The melting factor and threshold temperature for the snow routine were set to 2.5 and 0° respectively (both proved to be insensitive when within reasonable limits), while the shape parameter m of the exponential decline of the saturated hydraulic conductivity was fix for every grid cell and calculated according to section 4.3.

The Monte Carlo simulations were performed with a warm-up period of 7200 h (300 days, 01.01.1997 - 28.10.1997), a calibration period of 7200 h (29.10.1997 - 23.08.1998) and validation period of 7200 h (24.08.1998 - 19.06.1999).

### 4.5.1 Scatter Plots for modeled $E_{act}$

The scatter plots for the model configuration where $E_{act}$ is derived from the relative water content of the unsaturated zone are given in Fig. 4.8 and Fig. 4.9. The two right colums of Fig. 4.8 and the entire Fig. 4.9 show parameter spaces where all runs that exceed a threshold value for RMSE are drawn in red. This enables the evaluation of model efficiencies by taking into account both the isotope transport and runoff generation. The choice of the threshold value ensures that the 200 best parameter sets with regard to RMSE are included. The threshold value for acceptable values of $RMSE_{\delta^{18}O}$ of the model configuration in stake here accounts for 0.6145.

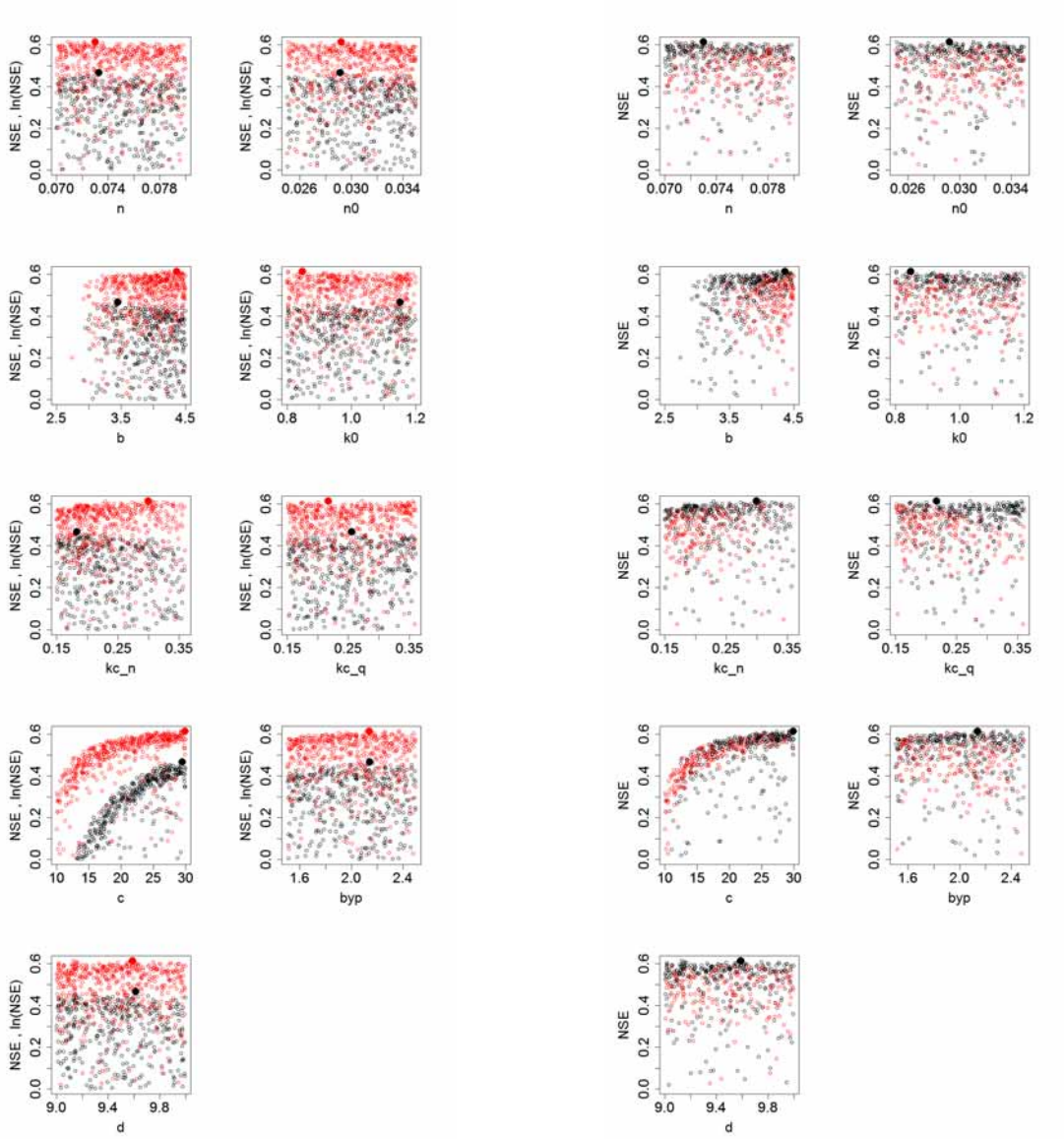


**Figure 4.8:** The two colums on the left show the parameter space with respect to NSE (red dots) and ln (NSE) (black dots). The two colums on the right show the parameter space with respect to only NSE and all runs having an acceptable $RMSE_{\delta^{18}O}$ drawn in red. Large dots mark position of highest likelihood measure.

The significantly lower maximum values of ln(NSE) compared to NSE reveal difficulties in producing acceptable model efficiency with respect to low flow. For the total porosity, the drainable porosity, the saturated hydraulic conductivity of the quarternary deposits, the power exponent of the recharge function and the power exponent of the bypass flow function, the parameter values with good likelihood measures are in accordance for both NSE und ln(NSE). The scatter plots comparing the model efficiencies for runoff and isotope transport show that a good representation of the storage properties, i.e. an appreciable value for $RMSE_{\delta^{18}O}$, does not

automatically lead to high efficiencies concerning runoff. This becomes particularly obvious for the power exponent of the recharge function and the total porosity. They also demonstrate that for both NSE and ln(NSE) the parameter ranges with acceptable $RMSE_{\delta^{18}O}$ are more or less consistent.

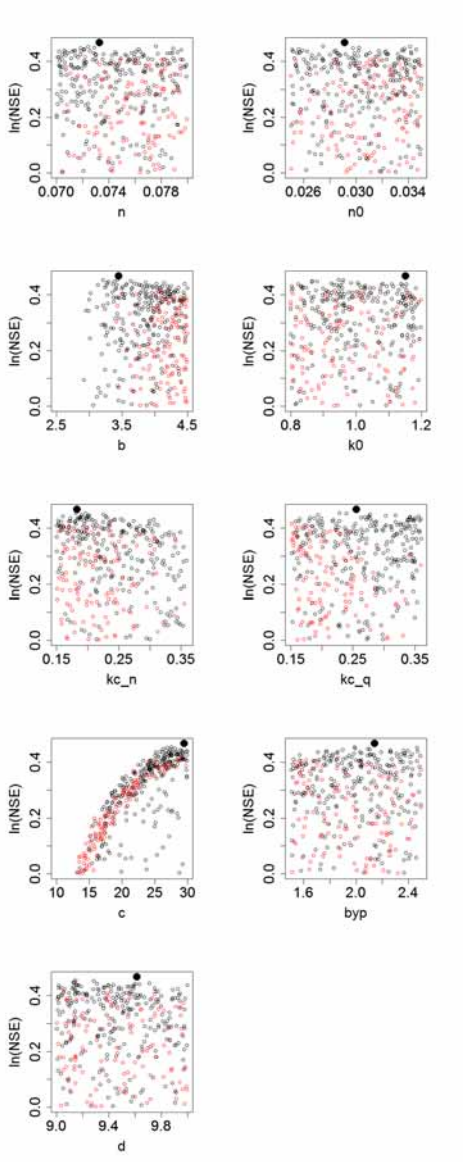


**Figure 4.9:** The parameter space with respect to ln (NSE) with all runs having an acceptable $RMSE_{\delta^{18}O}$ drawn in red. Large dots mark position of highest likelihood measure.

### 4.5.2 Scatter Plots for $E_{act} = E_{pot}$

The scatter plots for the model configuration with $E_{act} = E_{pot}$ are given in Fig. 4.10 and in Fig. 4.11. They are arranged in the same way as before. The threshold value

for an acceptable $RMSE_{\delta^{18}O}$ is again chosen by including the 200 best values and accounts for 0.6614.

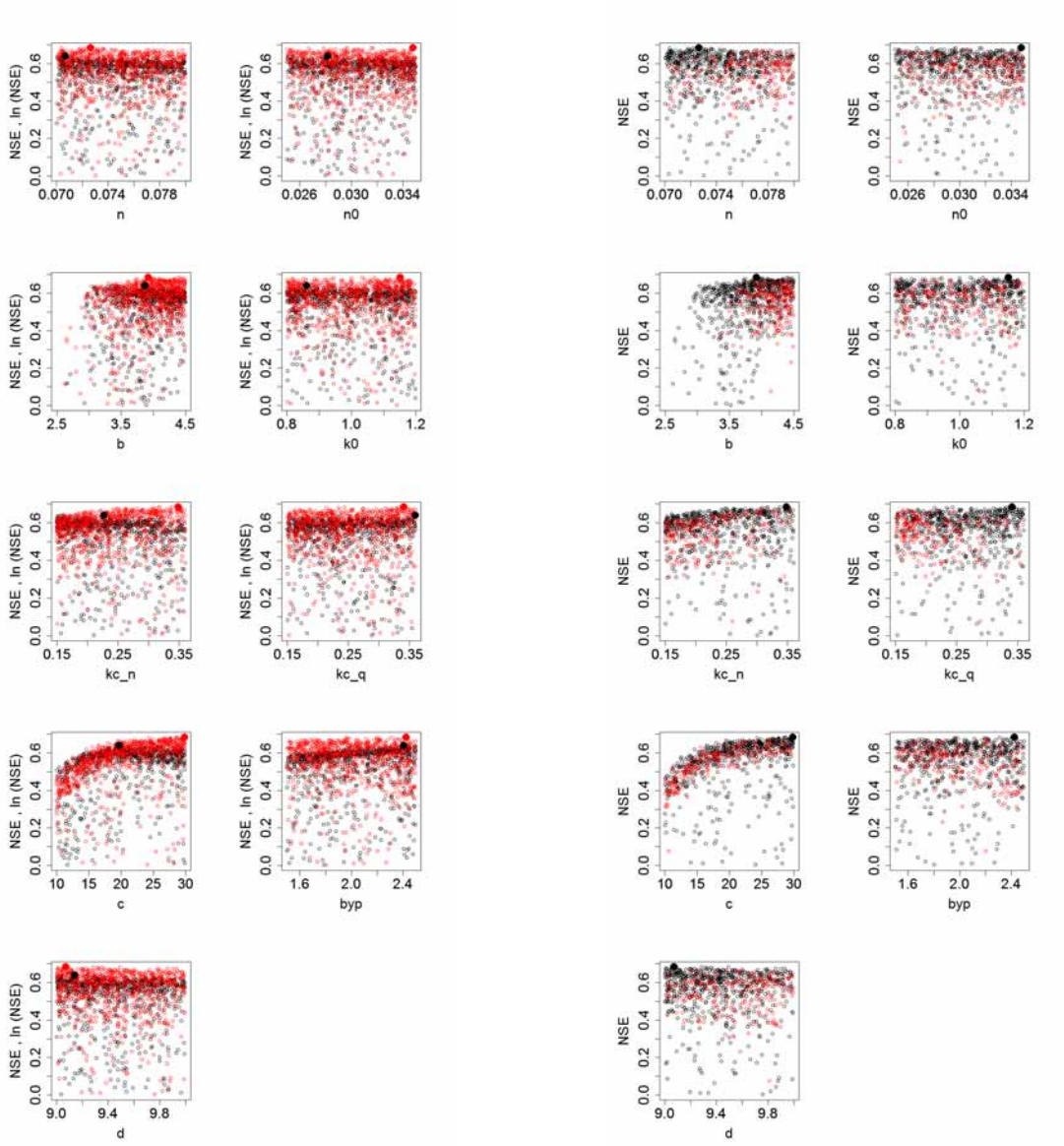


**Figure 4.10:** The two colums on the left show the parameter space with respect to NSE (red dots) and ln (NSE) (black dots). The two colums on the right show the parameter space with respect to only NSE and all runs having an acceptable $RMSE_{\delta^{18}O}$ drawn in red. Large dots mark position of highest likelihood measure.

Obviously the model performance concerning low-flow has significantly improved. The ln(NSE) reaches approximately the same efficiency-level as the NSE. With the exception of the drainable porosity, the saturated hydraulic conductivity at the soil surface and the saturated hydraulic conductivity of the “Nagelfluh” layer, there is a good agreement between NSE and ln(NSE) concerning the position of parameter sets with good likelihood values. Again, the acceptable runs with respect to

$RMSE_{\delta^{18}O}$ are not equally distributed as those with high efficiencies for runoff. This is particularly true for the total porosity and the saturated hydraulic conductivity of the quarternary deposits.

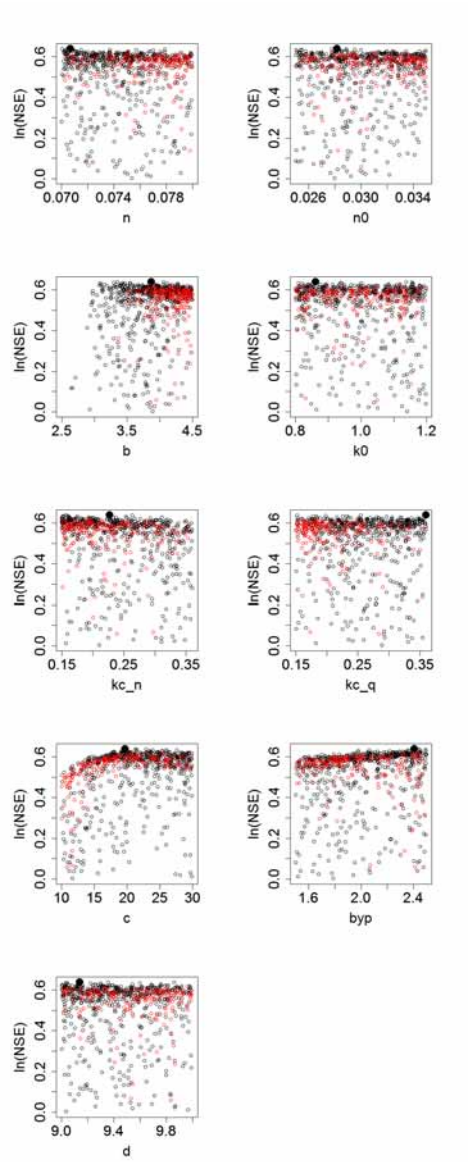


**Figure 4.11:** The parameter space with respect to ln (NSE) with all runs having an acceptable $RMSE_{\delta^{18}O}$ drawn in red. Large dots mark position of highest likelihood measure

### 4.5.3 Resulting Parameter Sets

As most appropriate parameter sets with respect to low-flow and storage properties for each model configuration those with the highest ln(NSE) of runs with an acceptable $RMSE_{\delta^{18}O}$ were chosen. They are given in Tab. 4.2.

**Table 4.2:** Calibrated parameter sets for both model configurations

| **name** | **description** | **min.** | **max.** | **optimum** (modeled $E_{act}$) | **optimum** ($E_{act}$=$E_{pot}$) |
|---|---|---|---|---|---|
| n | total porosity | 0.07 [-] | 0.08 [-] | 0.073 [-] | 0.075 [-] |
| n0 | drainable porosity at soil surface | 0.025 [-] | 0.035 [-] | 0.032 [-] | 0.028 [-] |
| b | shape parameter of exponential depth function of drainable porosity | 2.5 [m] | 4.5 [m] | 3.66 [m] | 4.19 [m] |
| k0 | saturated k-value at soil surface | 0.8 [m/h] | 1.2 [m/h] | 1.04 [m/h] | 0.81 [m/h] |
| kc_n | saturated k-value of "Nagelfluh" | 0.15 [m/h] | 0.36 [m/h] | 0.17 [m/h] | 0.19 [m/h] |
| kc_q | saturated k-value of quarternary deposits | 0.15 [m/h] | 0.36 [m/h] | 0.16 [m/h] | 0.18 [m/h] |
| c | exponent of recharge function | 10 [-] | 30 [-] | 27.38 [-] | 23.39 [-] |
| byp | exponent of bypass function | 1.5 [-] | 2.5 [-] | 2.38 [-] | 2.40 [-] |
| d | total thickness of simulated layer | 9 [m] | 10 [m] | 9.32 [m] | 9.79 [m] |

The corresponding efficiency measures can be found in Tab. 4.3. In contrast to the other likelihood measures ln(NSE) is higher for the validation period than for the calibration period. A reason might be the long phase of high runoff during the calibration period because the model is better able to simulate low-flow than high discharges. However, it seems that the model configuration with $E_{act} = E_{pot}$ is able to reproduce flow recessions during periods of high runoff with more accuracy.

**Table 4.3:** Efficiency measures for the two model configurations

| Configuration | Calibration Period | | | Validation Period | | |
|---|---|---|---|---|---|---|
| | NSE | ln NSE) | $RMSE_{\delta^{18}O}$ | NSE | ln(NSE) | $RMSE_{\delta^{18}O}$ |
| Modeled $E_{act}$ | 0.56 | 0.42 | 0.614 | 0.51 | 0.63 | 1.09 |
| $E_{act} = E_{pot}$ | 0.59 | 0.62 | 0.652 | 0.48 | 0.69 | 1.20 |

### 4.5.4 Uncertainty Analysis

The model uncertainty with respect to runoff was determined by using the method of generalized likelihood uncertainty estimation (GLUE) which was developed by Beven and Binley (1992). It is based on the association of each parameter set with its likelihood measure, here NSE, and then the distinction between behavioural and non-behavioural parameter sets or simulations, respectively. This is done by choosing a threshold value of the likelihood measure subjectively that each acceptable simulation has to surpass. Confidence intervals for the simulated discharges, e.g. the 95 % confidence interval, are computed by arranging the simulated streamflows of all behavioural simulations for every timestep in ascending order and then using the 0.025 and the 0.975-quantile as lower und upper limits (Beven and Binley, 1992; Gattke, 2006). The result for the warm-up period and for the calibration period are given in Fig. 4.12.

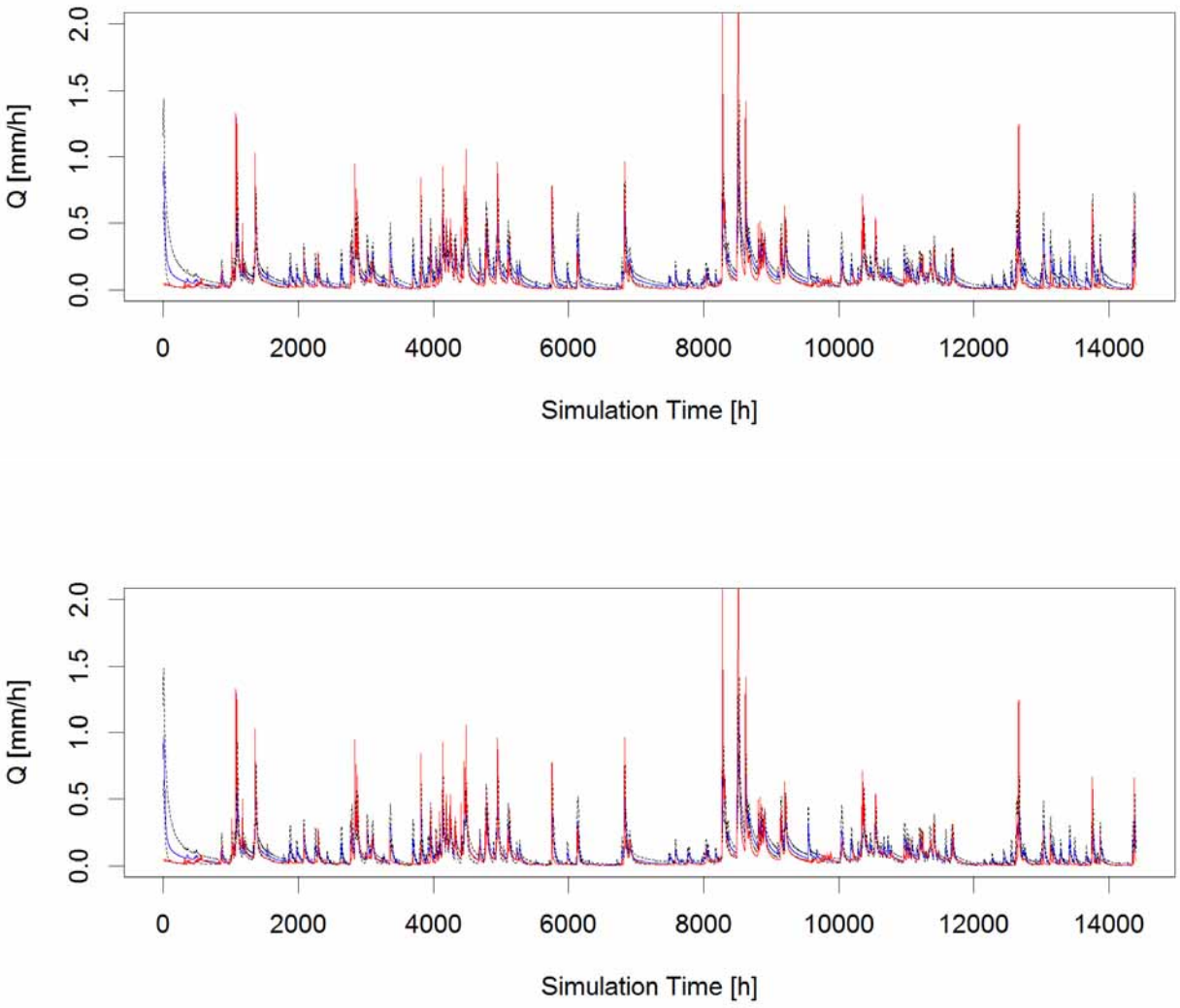


**Figure 4.12:** The upper plot shows the 95 % GLUE prediction limits (black dashed lines) for the model configuration with lower evaporation (threshold NSE = 0.4), the lower plot shows the same for the model configuration with $E_{act} = E_{pot}$ (threshold NSE = 0.5). The blue line is the median GLUE, while the red line represents the observed time series.

The 95 % prediction limits are quite similar for both model configurations, differences can mainly be observed at recession curves. There the median GLUE and the upper prediction limit often are signicantly higher for the model configuration with lower evaporation.

# 5 Results

## 5.1 Runoff

The modeled annual water balance for both model configurations is given in Tab. 5.1. A comparison of both water balances points out that the model configuration with less evaporation produces significantly more runoff.

**Table 5.1:** Modeled average annual water balance of the Rietholzbach catchment (simulation period 01.01.1997 - 26.08.2000).

| | Modeled $E_{act}$ | $E_{act} = E_{pot}$ |
|---|---|---|
| Precipitation | 1482 mm | 1482 mm |
| Runoff | 1114 mm | 1000 mm |
| Evaporation | 345 mm | 480 mm |

The modeled and observed time series of runoff are illustrated in Fig. 5.1.

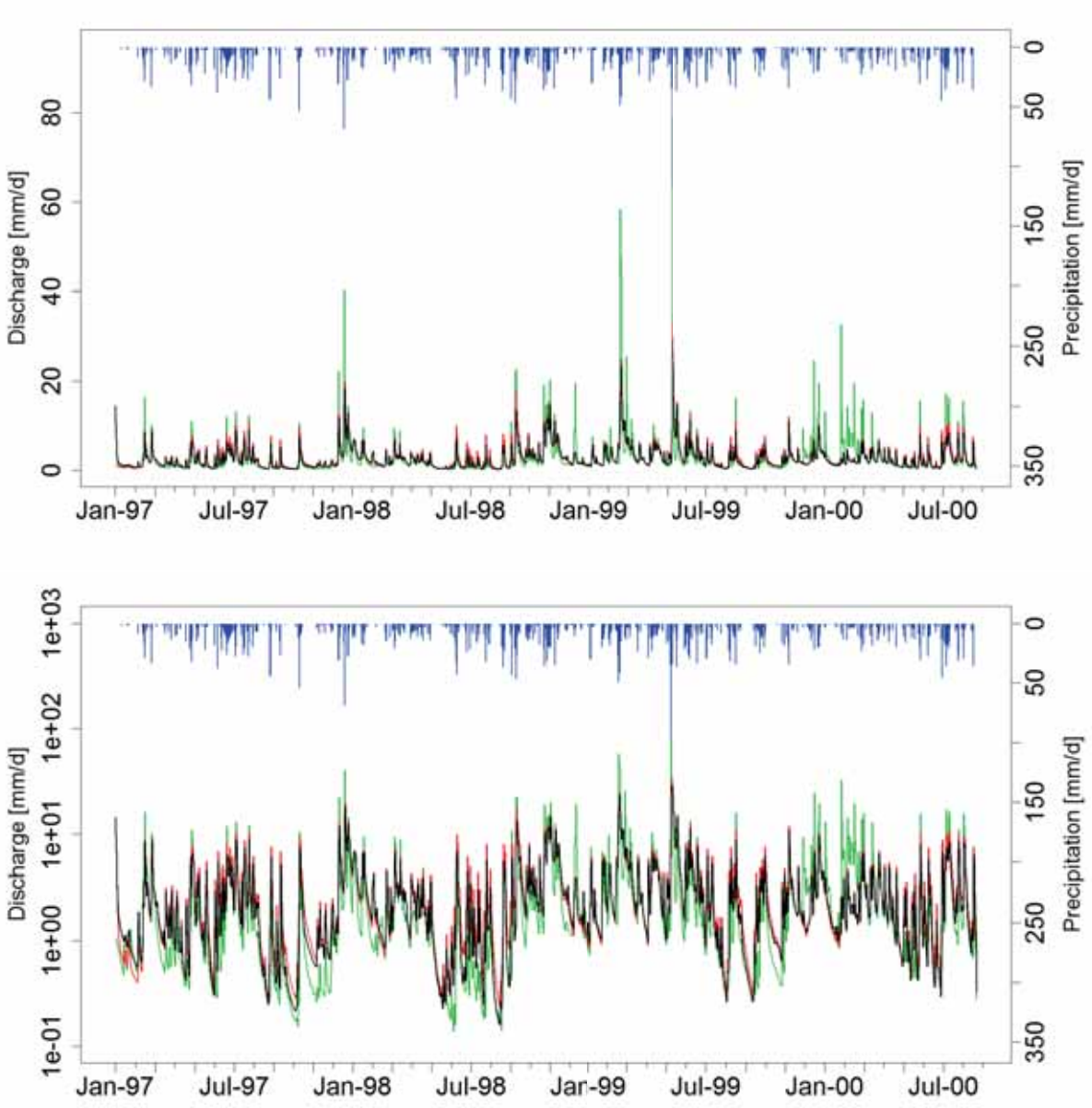


**Figure 5.1:** Modeled and observed runoff time series. In the lower plot discharge is given logarithmically. Observed runoff is represented by the green line, modeled runoff is represented by the red (modeled $E_{act}$) and green lines ($E_{act} = E_{pot}$). The precipitation is given as blue bars pointing downwards.

The model configuration with $E_{act} = E_{pot}$ is slightly more capable of reproducing appropriate low flows and recession curves, while it is inferior in terms of peak flows compared to the configuration with modeld $E_{act}$. Regardless of the model configuration there are difficulties in reproducing the extreme variability of the observed runoff and the very fast response to rainfall events which even occurs after longer periods of zero precipitation.

Fig. 5.2 shows the flow duration curves for observed and modeled discharges plotted logarithmically. The flow duration curves illustrate again what is suggested by the previous plots of discharge over time: The distribution of low-flows of the model with $E_{act} = E_{pot}$ is closer to the observed one than those of the other model configuration. However, in a mid-range of discharges at approximately Q30 - Q80, neither configuration is able to reproduce the distribution of observed values.

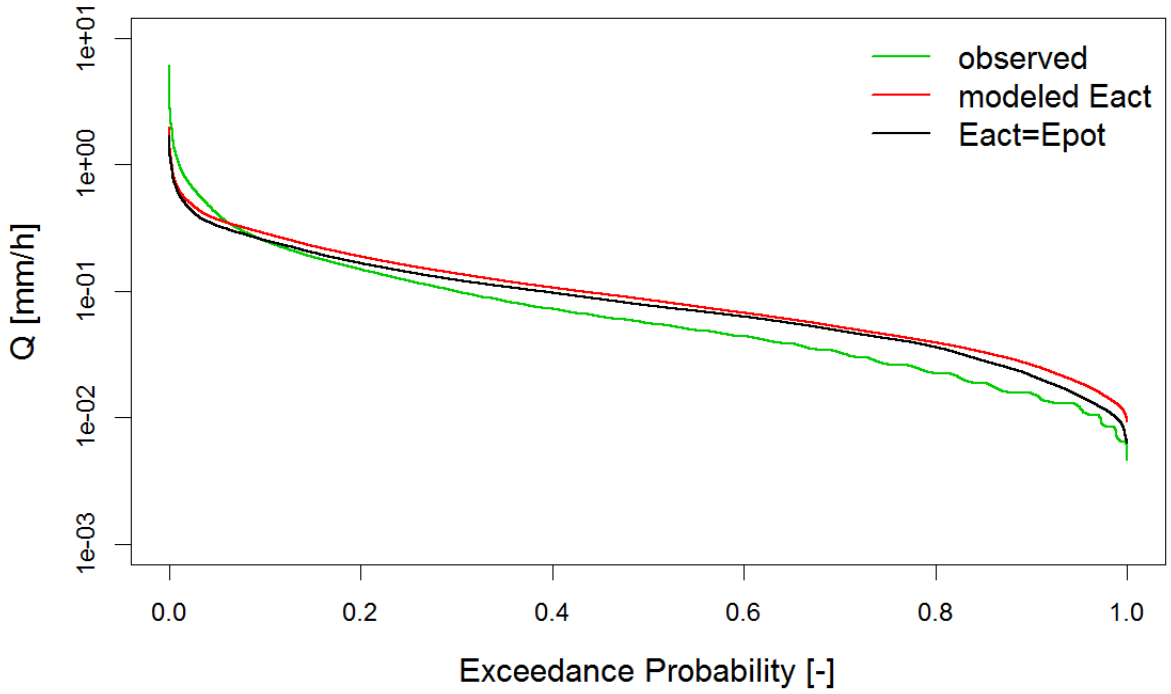


**Figure 5.2:** Flow duration curves for both observed and modeled discharges plotted logarithmically.

A recession curve analysis based on the method of plotting -dQ/dt vs. Q introduced by Brutsaert and Nieber (1977) has been performed. Rupp and Selker (2006) point out that the result of recession curve analyses by this method is strongly dependent on the chosen timestep and propose the use of a variable timestep. Nevertheless in this work a constant timestep of 24 hours has been used because no physically meaningful aquifer parameters are to be derived. The recession curve analysis here only serves as a visual comparison betwen modeled and observed data. It is given in Fig. 5.3.

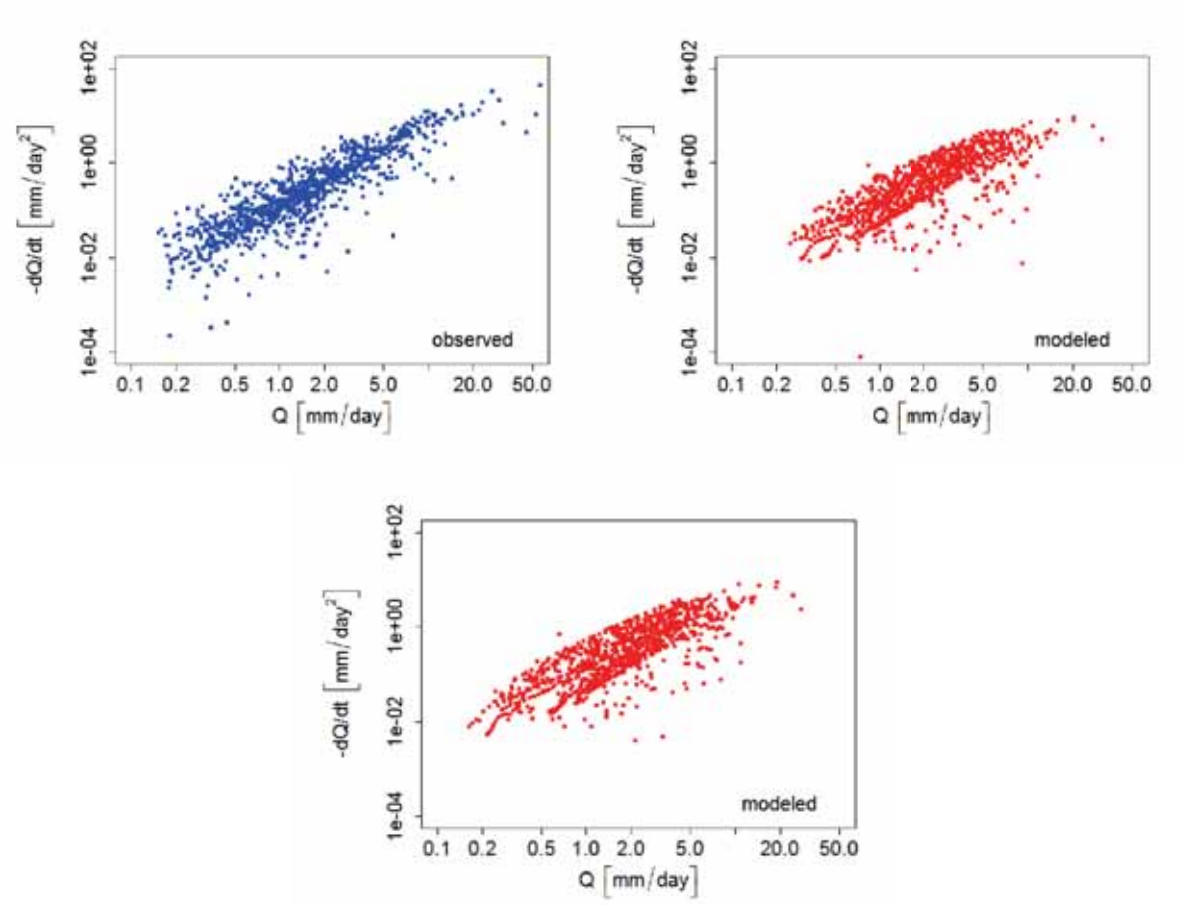


**Figure 5.3:** Flow recession curve analysis for observed discharge and both model configurations in log-log space. On the upper right hand side is the recession curve analysis for the low evaporation model, the lower plot is for the model configuration with higher evaporation.

Shape and slope of the scatter plots are in acceptable agreement with the observed data for both models. The model with $E_{act} = E_{pot}$ is better capable of reaching the lower limits of the observed data.

Relative errors of modeled to observed daily runoff against modeled daily runoff for both model configurations are illustrated in Fig. 5.4

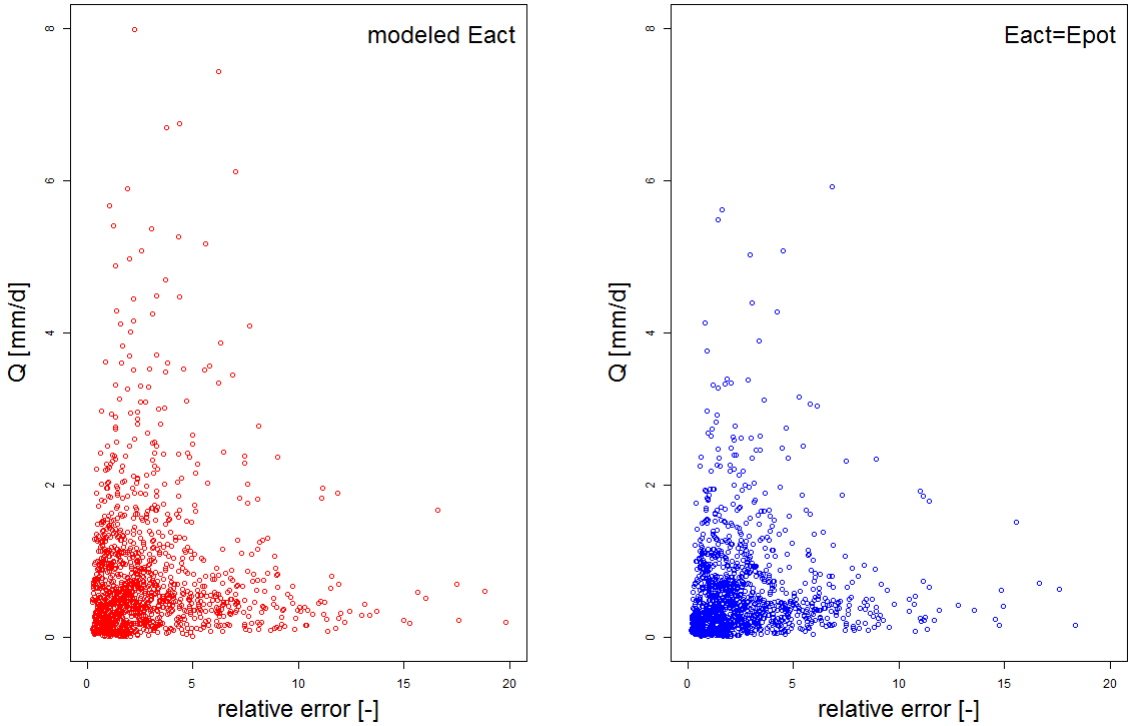


**Figure 5.4:** Relative error of modeled to observed runoff against modeled runoff for the model configuration with lower evaporation (left hand side) and higher evaporation (right hand side).

The shape of the scatter plots is quite similar for both model configurations. Concerning relative error, the performance of the higher evaporation model is again slightly better for low-flow than the performance of the model with evaporation calculated as fraction of unsaturated water content.

## 5.2 Isotope transport and modeled transit time

The result of isotope transport is plotted in Fig. 5.5. The modeled isotopic compositions in discharge show a stronger response to the isotope input delivered by precipitation than the observed isotopic compositions in discharge. Nevertheless the curves of modeled $\delta^{18}O$ in discharge for both models reflect quite well the trends of observed $\delta^{18}O$ in discharge.

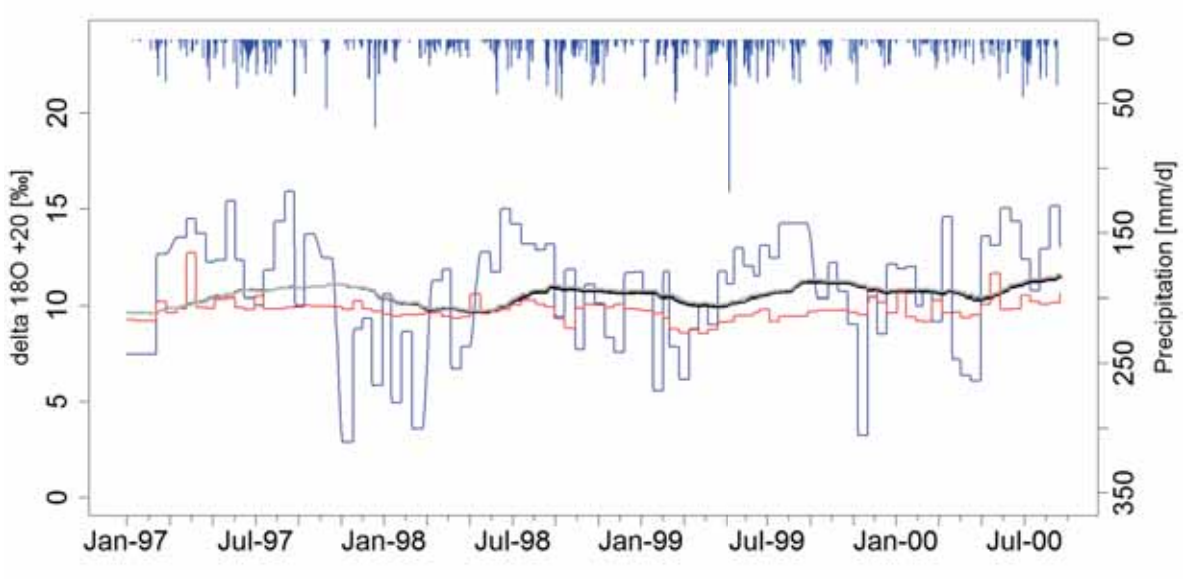


**Figure 5.5:** Times series of observed $\delta^{18}O$ in precipitation (blue line), observed $\delta^{18}O$ in discharge (red line), modeled $\delta^{18}O$ in discharge for the model configuration with lower evaporation (black line) and modeled $\delta^{18}O$ in discharge for the model configuration with $E_{act} = E_{pot}$ (grey line). The precipitation is given as blue bars pointing downwards.

Transit times were derived by performing a sudden Dirac impulse over the whole area. To investigate if there are differences in transit times for periods with high runoff or low-flow inputs were made at varying times. Transit times were determined for both model configurations. The results of the transit time modeling in terms of a mean transit time are given in Tab. 5.2.

**Table 5.2:** Mean transit times for both model configurations

| | Input on 06.01.1998 18:00 (high runoff period) | Input on 17.05.1998 18:00 (low-flow period) |
|---|---|---|
| Modeled $E_{act}$ | 143.1 days | 214.4 days |
| $E_{act} = E_{pot}$ | 139.8 days | 205.5 days |

The corresponding plots are given in Fig. 5.6 for the model configuration with lower evaporation and in Fig. 5.7 for the model configuration with $E_{act} = E_{pot}$.

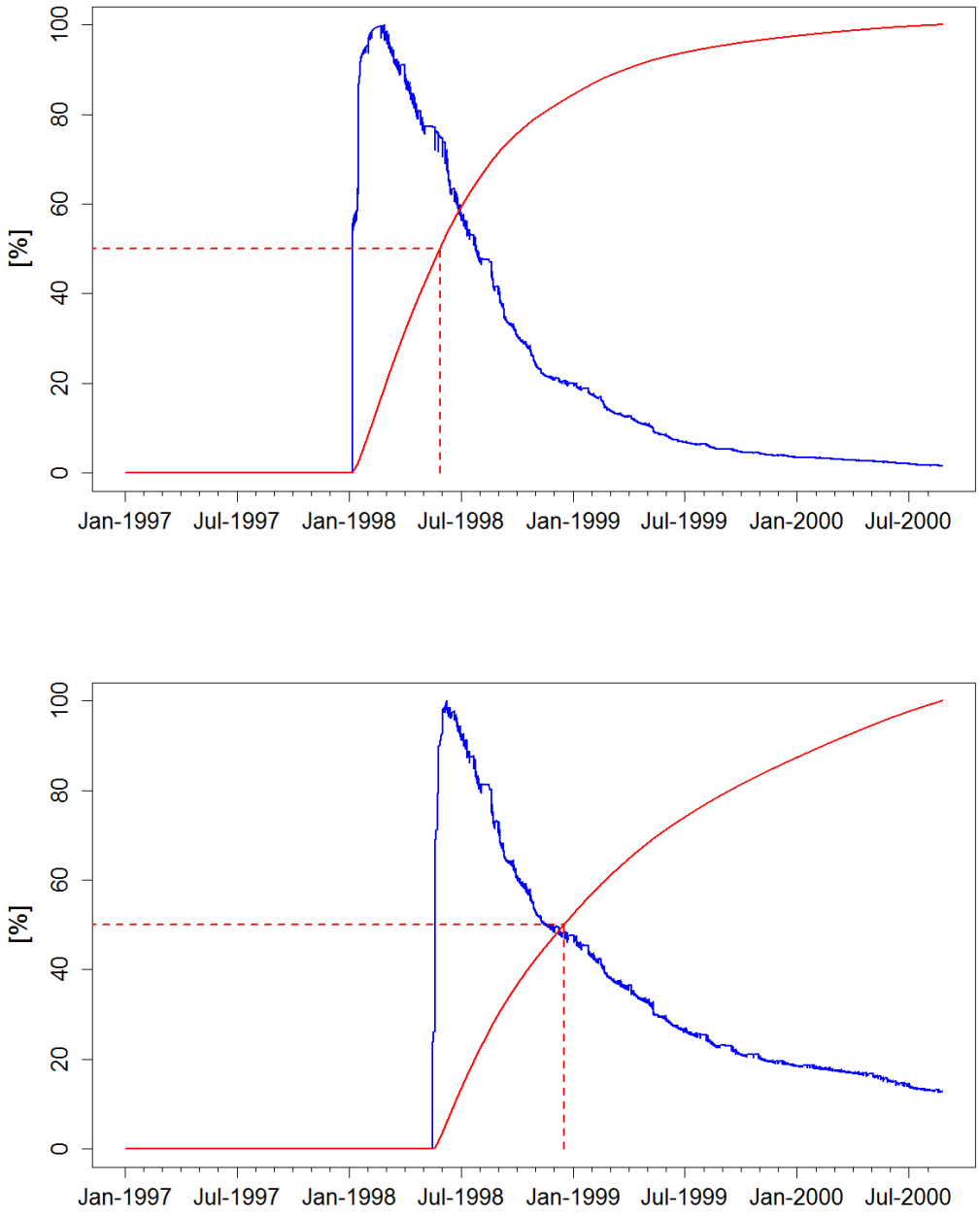


**Figure 5.6:** Normalised isotopic composition in discharge (blue line) produced by the model configuration with lower evaporation and cumulative sum of isotopic compositions (red line) for input during a period of high discharges (upper plot) and during a period of low-flow (lower plot). The dashed red line marks the mean transit time (cumulative sum = 50 % of maximum).

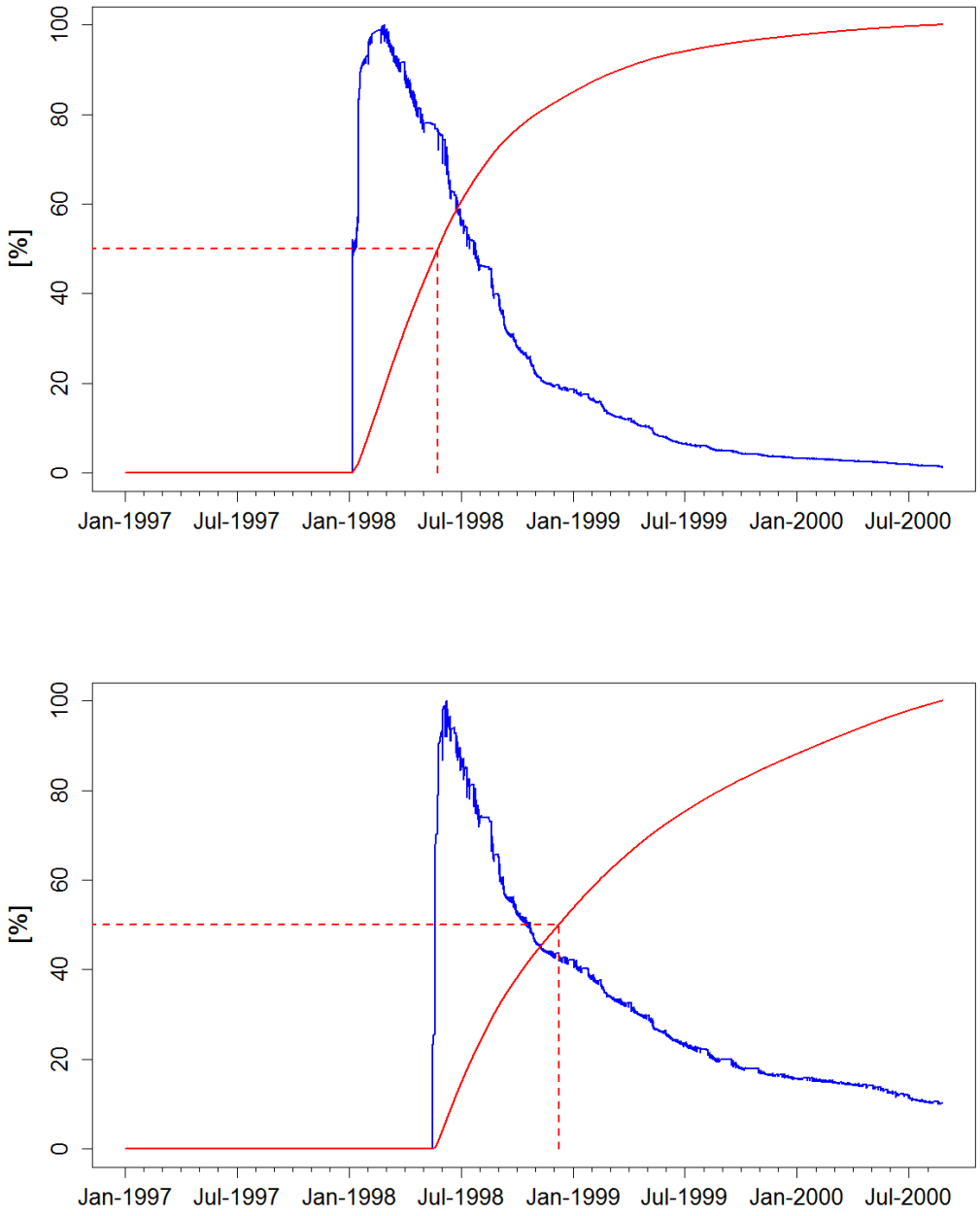


**Figure 5.7:** Normalised isotopic composition in discharge (blue line) produced by the model configuration with higher evaporation and cumulative sum of isotopic compositions (red line) for input during a period of high discharges (upper plot) and during a period of low-flow (lower plot). The dashed red lines mark the mean transit time (cumulative sum = 50 % of maximum).

The transit time modeling demonstrates the differences in mean transit time depending an flow regime. During periods of low-flow the mean transit time is signifcantly higher than during times of high discharges. The differences between both

model configuration are relatively small, with slightly shorter transit times for the model with $E_{act} = E_{pot}$.

## 5.3 Storage dynamics

The change in water content of the different storages for each model configuration is illustrated in Fig. 5.8. It reveals that during low-flows most of the water is stored in the unsaturated storage. The saturated storage is only filled as response to precipitation input when runoff is produced. As a result of the inversely proportional behaviour of saturated and unsaturated storage, the water volume contained in the total storage remains relatively constant over time. Runoff is not produced as a more or less constant portion of the total storage; instead, unsaturated zone is converted into saturated zone as a response to precipitation input.

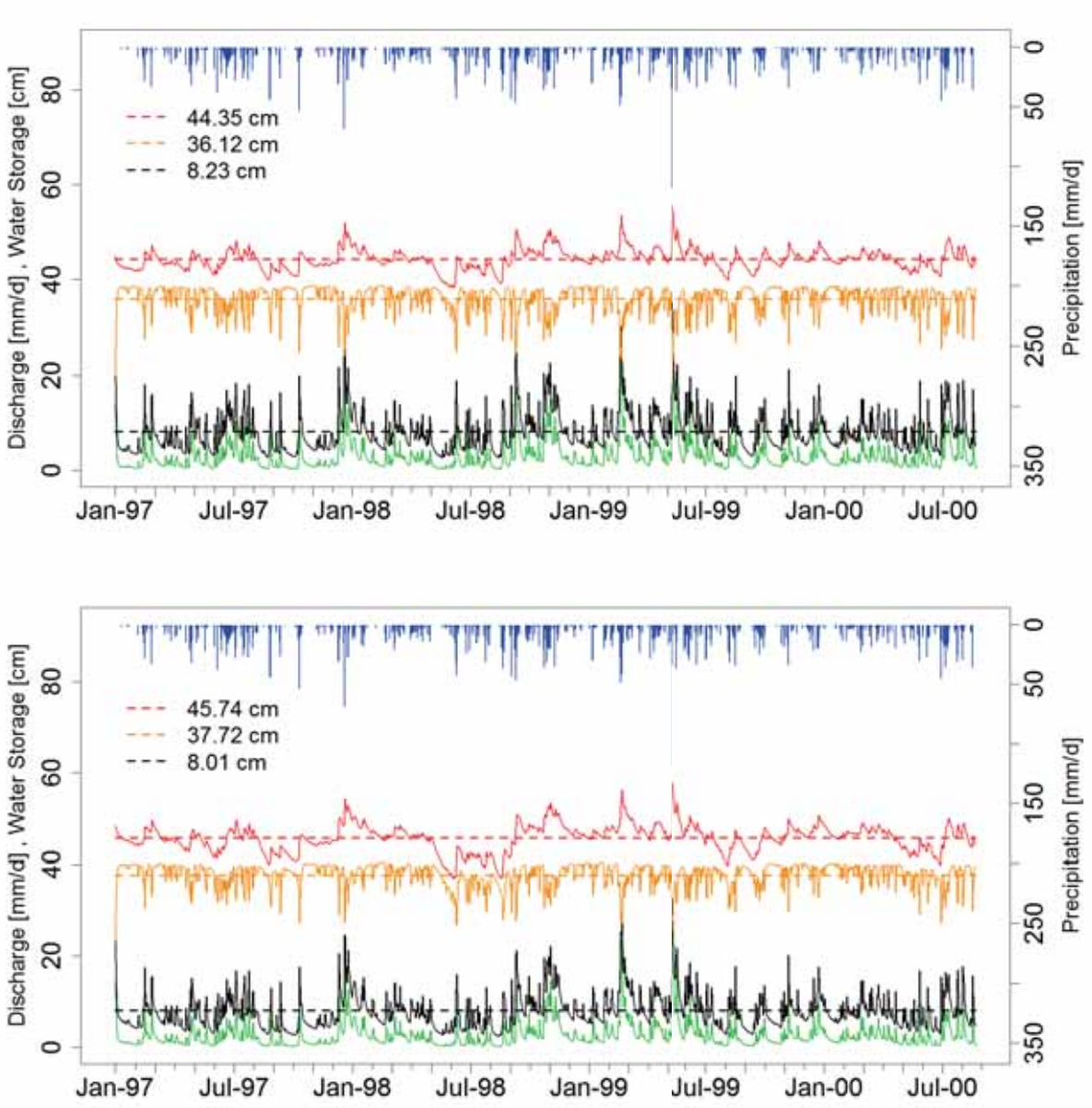


**Figure 5.8:** Water content over time of the total water storage (red lines), the unsaturated storage (orange lines) and the saturated storage (black lines) and discharge (green lines). The dashed horizontal lines represent the average water content of the corresponding storages. Their average water contents are given in cm in the upper left corner of each plot. The upper plot is for the model configuration with lower evaporation, the lower plot is for the model configuration with $E_{act} = E_{pot}$.

A comparison of the two model configurations shows that there is little difference in total storage capacity, but the proportions between the storages differ. In relation to the total storage more water is stored in the unsaturated zone and less in the saturated zone when the model is configured with $E_{act} = E_{pot}$. The temporal dynamic of the storages is also illustrated in Fig. 5.9. It becomes obvious that the dynamic in

change of storage is far higher for the saturated and unsaturated zones than for the total storage. Furthermore, even at low values of daily discharge the water content of the total storage remains relatively constant and never falls below 300 mm.

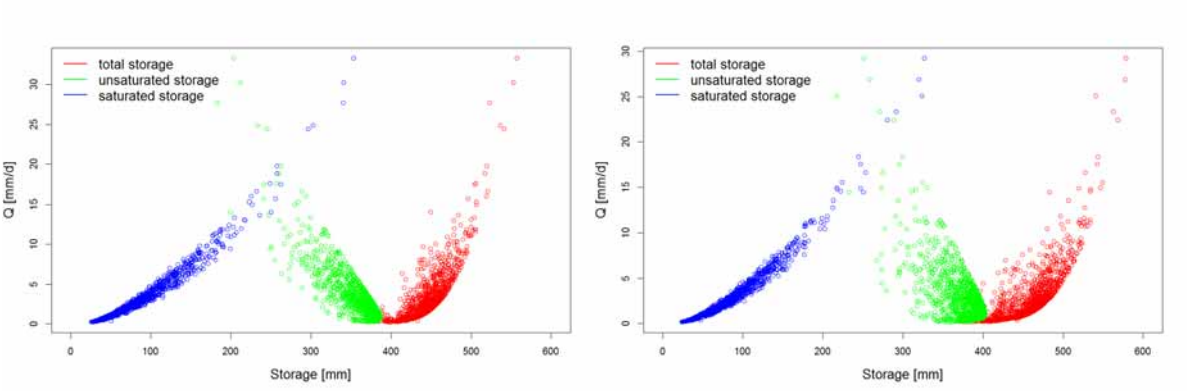


**Figure 5.9:** Scatter plot of storage water content versus runoff. Saturated storage is coloured blue, unsaturated storage is coloured green, total storage is coloured red. The upper plot is for low evaporation, the lower plot is for high evaporation.

The development of observed and modeled water table depth below ground level over time is shown in Fig. 5.10 for each model configuration.

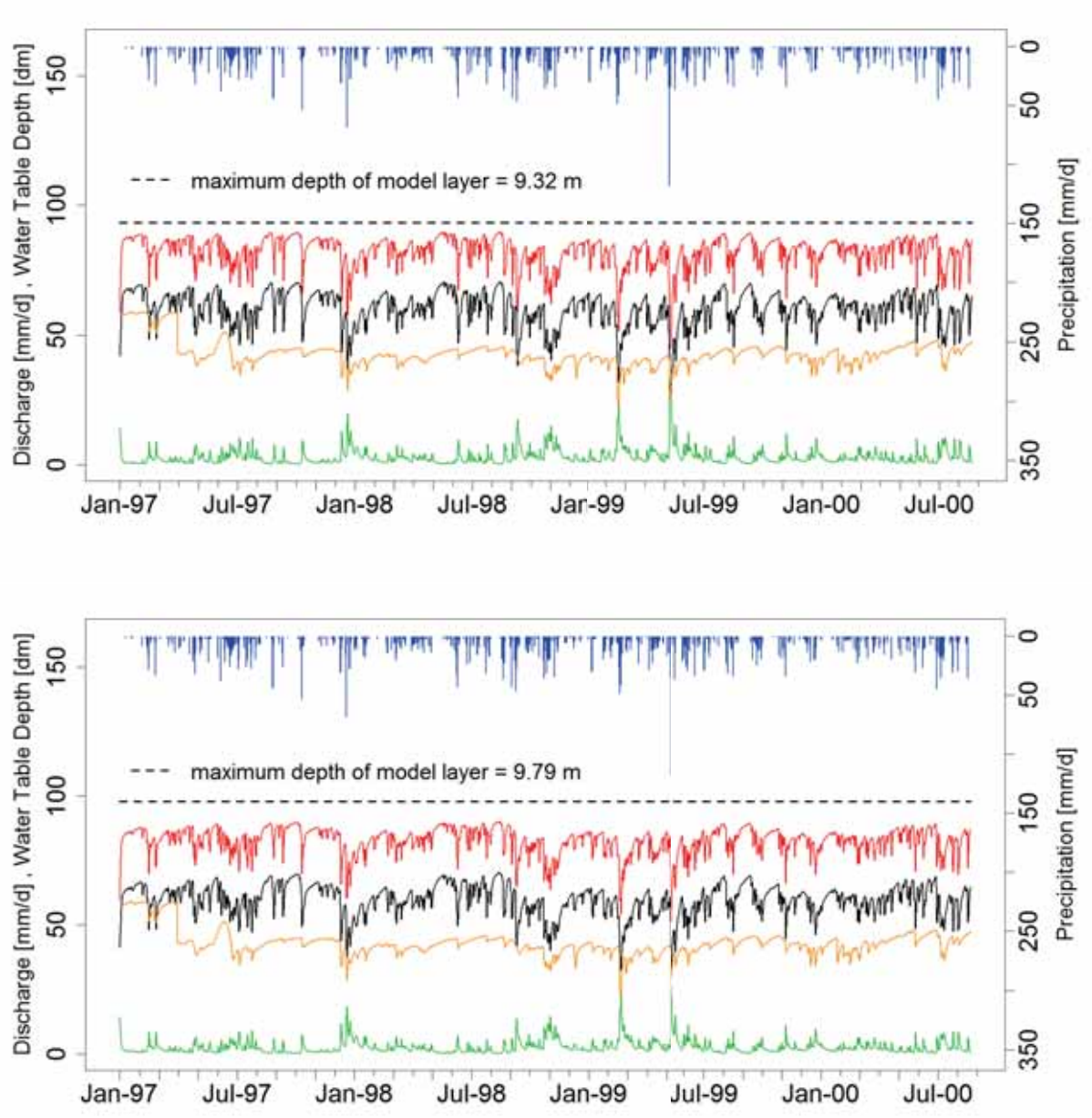


**Figure 5.10:** Water table depths below ground level for model configuration with higher evaporation (lower plot) and lower evaporation (upper plot). Water table depths are given as mean value for the whole model domain (red lines), as mean value of the water table depths in cells assigned to the quarternary valley sediments (black) and as observed (observation hole B1) values at Buel climate station (orange values). The dashed horizontal lines mark the position of maximum layer depths. The discharge is given as a green line.

In comparison to the observed values the water table depths are too high for both model configurations. They also show a higher variability and faster changes than the observed water table depth. The significantly higher modeled water table depths at the valley bottom reveal that they are not evenly spread over the catchment. This is also illustrated by Fig. 5.11. Highest water table depths are always distributed

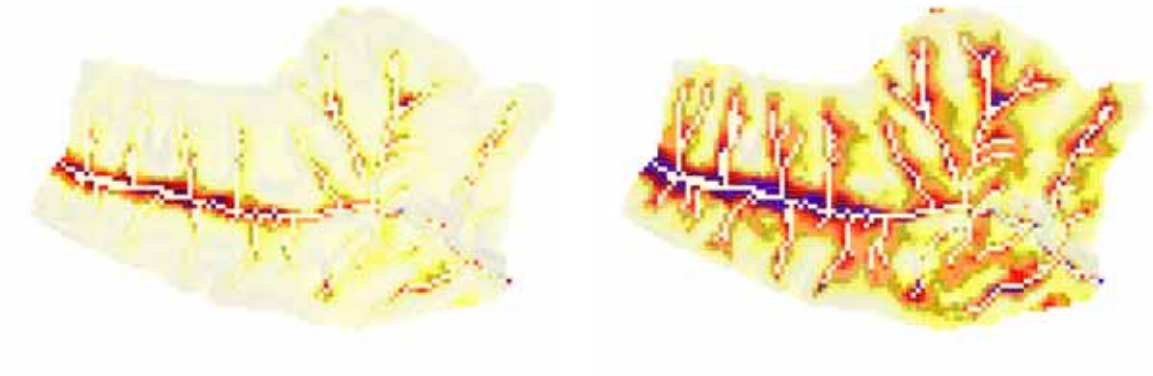

**Figure 5.11:** Modeled spatial distribution of saturation depths. Areas coloured pale yellow have highest saturation depth, areas coloured blue have lowest saturation depth. The left graphic is for low-flow conditions, the right for a period of high runoff, but not peakflow.

along channel cells in the valley bottom, especially in regions with relatively flat topography.

# 6 Discussion

## 6.1 Model plausibility

With respect to runoff and especially with respect to low-flow the model is mostly able to reproduce acceptable values. A closer look at the modeled runoff time series reveals some unrealistic sudden peak flows in winter (e.g. end of January 1998) in phases with a sudden onset of temperatures above 0°. It seems the snow routine is only partly able to reproduce appropriate effects of snow melt on discharge. In this thesis the parametrisation of the snow routine has been predeterminded (see section 4.5), but it may be sensible to put more emphasis on the snow routine in future modeling with HillVi.

The flow mechanisms leading to runoff are in good agreement with what can be expected in reality as it is demonstrated by the values given in Tab. 6.1. As in reality, saturated subsurface flow routed into the Rietholzbach creek and its tributaries is the dominant flow process. The runoff due to exceeding cell storages could be considered to be saturation excess overland flow, which is probable to occur in the upper parts of the Rietholzbach catchment described as wetland in literature (Kuhn, 1980).

Model runs where the actual evaporation was forced to equal the potential evaporation systematically had a higher model efficiency and produced a more plausible water balance. This reveals some structural problems of the model. Modeling a plau-

**Table 6.1:** Processes producing runoff

| runoff process | modeled $E_{act}$ | $E_{act} = E_{pot}$ |
|---|---|---|
| SSF | 1103 mm | 991 mm |
| exceeding cell storages | 11 mm | 9 mm |

sible actual evaporation which would be close to the potential evaporation, as can be expected in a catchment with a permanently high water availabilty, would require the ratio of actual water content of the unsaturated storage and its maximum water content ($S_{un}/S_{max,un}$) to be close to 1 for most of the time. In fact, this ratio averagely accounted for about 0.6 in model runs. It seems that the modeled soil layer is not able to reproduce the soil water retention characteristics that occur in reality.

Generally it should be noted that the soil layer implemented in this modeling is not a good representation of reality in terms of total porosity. The total porosity for this modeling has been chosen according to values of the geological units that occur in the Rietholzbach catchment. This is acceptable in terms of total storage capacities but, while not having implemented a depth function of total porosity, it leads to a significant underestimation of the soil layer's total porosity.

Another problem concerning plausibility seem to be the modeled goundwater levels, which appear far too low compared to observed values. This usually would indicate a general lack of water. But, in contrast to common expectations, the modeled dynamics of the groundwater table are not a first order control of the total water storage (see Fig. 5.8). According to this, low goundwater levels do not generally represent a low water availability. Under consideration of the extremely small drainable porosities (which even at the soil surface only amount to about 3 % ) in depth one could even speak of the unsaturated zone to be "semi-saturated" and a representation of higher groundwater levels. In summary, the low watertables do not indicate a general underestimation of storage water compared to reality.

## 6.2 Transit time

Compared to former transit time estimations (Vitvar and Balderer, 1997; Vitvar et al., 1999) the modeled mean transit time is lower, but still within reasonable limits what is a good indication that the model renders an acceptable representation of storage properties. This is confirmed by the plausible modeled variation of transit times depending on high or low-flow. The lower mean transit times compared to former estimations could be explained by the simplifying structure of the model concerning the complex geology and soil distribution of the catchment. Another reason might be the assumption of complete mixing in the saturated and the unsaturated zone, which has a large effect on transit time as it is revealed by comparisons with models implementing an "active" and a "dead" storage compartment (Fenicia et al., 2010).

## 6.3 Hydrological droughts in the Rietholzbach catchment?

According to the modeling results runoff is mainly controlled by the water table development and not primarily by the total storage water. Even in periods of extreme low-flow ( < Q90) the modeled water storages are far from being completely drained 5.9. Tallaksen (2007) indentifies hydrological droughts as water scarcity in both runoff and groundwater storage. With respect to this definition the resilience of the Rietholzbach catchment to longer periods of low precipitation and high evaporational loss is relatively high concerning the availability of groundwater, but far lower concerning runoff.

# 7 References

Balderer, W. (1982). Hydrogeologie der Oberen Süsswassermolasse im Einzugsgebiet des Aubaches (Schweiz). *Steir. Beitr. Hydrogeologie 34/35*, 15–54.

Beven, K. and A. Binley (1992). The future of distributed models: Model calibration and uncertainty prediction. *Hydrological Processes 6*(3), 279–298.

Bohrer, M. (1998). Räumlich differenzierte Erfassung der Einzugsgebietskennwerte und Modellierung des Wasserhaushalts im Rietholzbachgebiet unter Nutzung eines GIS.

Brutsaert, W. and J. Nieber (1977). Regionalized drought flow hydrgraphs from a mature glaciated plateau. *Water Resources Research 13*, 637–643.

Buttle, J. M. and D. J. McDonald (2002, 05). Coupled vertical and lateral preferential flow on a forested slope. *Water Resour. Res. 38*(5).

DVWK (1996). Ermittlung der Verdunstung von Land- und Wasseroberflächen. *DVWK-Merkblätter zur Wasserwirtschaft 238*.

Fenicia, F., S. Wrede, D. Kavetski, L. Pfister, L. Hoffmann, H. H. G. Savenije, and J. J. McDonnell (2010). Assessing the impact of mixing assumptions on the estimation of streamwater mean residence time. *Hydrological Processes 24*(12), 1730–1741.

Freeze, R. and J. Cherry (1979). *Groundwater*. Prentice Hall, Englewood Cliffs, NJ.

Gascuel-Odoux, C., M. Weiler, and J. Molenat (2010). Effect of the spatial distribution of physical aquifer properties on modelled water table depth and stream discharge in a headwater catchment. *Hydrology and Earth System Sciences 14*(7), 1179–1194.

Gattke, C. (2006). *Modellvergleiche zur Untersuchung struktureller Unsicherheiten - Anwendung objektorientierter Methoden in der hydrologischen Modellierung*. Ph. D. thesis, Ruhr-Universität Bochum.

Germann, P. (1983). Untersuchungen über den Bodenwasserhaushalt im hydrologischen Einzugsgebiet Rietholzbach, 135 Seiten, Nr. 51 Mitteilungen der Versuchsanstalt für Wasserbau, Hydrologie und Glaziologie an der Eidgenössischen Technischen Hochschule Zürich. Hrsg.: Prof. Dr. D. Vischer. *Zeitschrift für Pflanzenernährung und Bodenkunde 146*(1).

Gurtz, J., S. Badertscher, C. Milzow, U. Moser, K. Schroff, R. Stoeckli, I. Völksch, and M. Zingg (2006). Auswertung der Messreihen der meteorologischen und hydrologischen Variablen im Forschungsgebiet Rietholzbach für den 30-jährigen Beobachtungszeitraum 1976-2005 mit besonderer Berücksichtigung des Trockensommers 2003.

Gurtz, J., M. Zappa, K. Jasper, H. Lang, M. Verbunt, A. Badoux, and T. Vitvar (2003). A comparative study in modelling runoff and its components in two mountainous catchments. *Hydrological Processes 17*(2), 297–311.

Haas, J. (2009). Concepts for Network Structures on Hillslopes.

Hirzel, G. (2009). Detecting and Measuring Overland Flow in the Eschibach Catchment, Ossingen, Switzerland.

Hisdal, H. and L. Tallaksen (2000). Drought Event Definition.

König, P. (1994). *Abflussprozesse in einem kleinen voralpinen Einzugsgebiet*. Ph. D. thesis, Zürcher Geographische Schriften, 58.

König, P., H. Lang, and R. Schwarze (1994). On the runoff formation in the small pre-alpine research basin Rietholzbach. *IAHS Publication* (221).

Krause, K.-H. (2000). *Die geologisch-hydrogeologische Situation im Jung- und Altmoränengebiet des Andechser Höhenrückens zwischen Ammer- und Würmsee und in der nördlich angrenzenden Wurzelzone der westlichen Münchener Schotterebene (Oberbayern)*. Ph. D. thesis, Technische Universität München.

Kuhn, H. (1980). Bodenkartierung Hydrex.

Leaney, F., K. Smettem, and D. Chittleborough (1993). Estimating the contribution of preferential flow to subsurface runoff from a hillslope using deuterium and chloride. *Journal of Hydrology 147*(1-4), 83 – 103.

McDonnell, J. J. (1990). A Rationale for Old Water Discharge Through Macropores in a Steep, Humid Catchment. *Water Resour. Res. 26*(11), 2821–2832.

McGlynn, B. L., J. J. McDonnel, and D. D. Brammer (2002). A review of the evolving perceptual model of hillslope flowpaths at the Maimai catchments, New Zealand. *Journal of Hydrology 257*(1-4), 1 – 26.

McGuire, K., M. Weiler, and J. J. McDonnell (2007). Integrating tracer experiments with modeling to assess runoff processes and water transit times. *Advances in Water Resources 30*, 824 – 837.

Nash, J. and J. Sutcliffe (1970). River flow forecasting through conceptual models part I – A discussion of principles. *Journal of Hydrology 10*(3), 282 – 290.

OCCC (2007). Hitzesommer 2003. *Synthesebericht*.

Penman, H. L. (1948). Natural evaporation from open water, bare soil and grass. *Proceedings of the Royal Society of London. Series A, Mathematical and Physical Sciences 193*(1032), pp. 120–145.

Refsgaard, J. C. (1997). Parameterisation, calibration and validation of distributed hydrological models. *Journal of Hydrology 198*(1-4), 69 – 97.

Rupp, D. E. and J. S. Selker (2006). Information, artifacts, and noise in dQ/dt vs. Q recession analysis. *Advances in Water Resources 29*(2), 154 – 160.

Tallaksen, L. M. (2007). Key Aspects of low flow and drought.

Vitvar, T. (1998). *Water Residence Times and Runoff Generation in a Small Prealpine Catchment*. Ph. D. thesis, Geographisches Institut der Universität Zürich.

Vitvar, T. and W. Balderer (1997). Estimation of mean water residence times and runoff generation by180 measurements in a Pre-Alpine catchment (Rietholzbach, Eastern Switzerland). *Applied Geochemistry 12*(6), 787 – 796.

Vitvar, T., J. Gurtz, H. Lang, C. Leibundgut, J. McDonnell, and G. Schultz (1999). Application of GIS-based distributed hydrological modelling for estimation of water residence times in the small Swiss pre-alpine catchment Rietholzbach.

Walter, H. and H. Lieth (1960). *Klimadiagramm Weltatlas*. G. Fischer, Jena.

Weiler, M. and J. McDonnell (2004). Virtual experiments: a new approach for improving process conceptualization in hillslope hydrology. *Journal of Hydrology 285*(1-4), 3 – 18.

Weiler, M. and J. J. McDonnell (2006). Testing nutrient flushing hypotheses at the hillslope scale: A virtual experiment approach. *Journal of Hydrology 319*(1-4), 339 – 356.

Weiler, M. and J. J. McDonnell (2007). Conceptualizing lateral preferential flow and flow networks and simulating the effects on gauged and ungauged hillslopes. *Water Resources Research 43*(3), 1–13.

Weiler, M., T. Uchida, and J. McDonnell (2003). Connectivity due to preferential flow controls water flow and solute transport at the hillslope scale. In *Proceedings of MODSIM 2003*.

Wigmosta, M. and D. Lettenmaier (1999, January). A comparison of simplified methods for routing topographically driven subsurface flow. *Water Resources Research 35*(1), 255–264.

Wigmosta, M. S., L. W. Vail, and D. P. Lettenmaier (1994). A distributed hydrology-vegetation model for complex terrain. *Water Resour. Res. 30*(6), 1665–1679.

# 8 Appendix 1

## Calculation of potential evaporation

The Penman approach for grassland (Penman, 1948) is calculated with (all following formulas are from DVWK, 1996):

$$E_{pot} = \frac{\Delta \cdot EH + \gamma \cdot f(v) \cdot (e_s - e_a)}{\Delta + \gamma} \tag{8.1}$$

Here, $E_{pot}$ is the potential Evaporation, $\Delta$ is the gradient of the saturated vapour pressure curve, EH is the net radiation equivalent, $\gamma$ is the psychrometer constant, f(v) is the wind function, $e_s$ is the saturated vapour pressure and $e_a$ is the vapour pressure. $\Delta$ is derived from

$$\Delta = e_s \cdot \frac{4032}{(237 + T)^2} \tag{8.2}$$

with T being the air temperature. EH is calculated with

$$EH = \left( \frac{RG \cdot (1 - r) - I}{28.3} \right) \tag{8.3}$$

where RG is the measured global radiation, r is albedo and I is the effectively reflected radiation. Albedo for different types of soil and vegetation is illustrated in Tab. 8.1. For the Rietholzbach catchment an albedo of 15 % has been estimated. The reflected radiation I is given by

$$I = 5.67 \cdot 10^{-8} \cdot (T + 273)^4 \cdot (0.56 - 0.08 \cdot \sqrt{e_a}) \cdot (0.1 + 0.9 \cdot s/S) \tag{8.4}$$

with T being the air temperature, $e_a$ the vapour pressure and s/S the quotient of recorded daily duration of sunshine and maximal daily duration of sunshine. Because there was no data for sunshine duration available it has been recalculated from recorded global radiation by

$$RG = (0.19 + 0.55 \cdot s/S) \cdot RE \tag{8.5}$$

where RG is global radiation and RE is extraterrestrial radiation. Values for RE depending on latitude are given in Tab. 8.2. Those for a northern latitude of 47° have been chosen for the Rietholzbach.

**Table 8.1:** Albedo for different soils and types of vegetation (DVWK, 1996).

| | | |
|---|---|---|
| Vegetationslose | dunkle Böden | 5 – 15 |
| Böden: | trockene Lehmböden | 20 – 35 |
| | graue Böden | 20 – 35 |
| | trockene, helle Sandböden | 25 – 45 |
| Bewachsene | Wüsten | 30 |
| Böden: | | |
| | Weizenfeld | 10 –25 |
| | Wiese | 15 – 25 |
| | Trockene Steppe | 20 – 30 |
| | Tundra und Laubwald | 15 – 20 |

**Table 8.2:** Extraterrestrial radiation depending on latitude (DVWK, 1996).

| Geogr. Breite | Jan | Feb | Mär | Apr | Mai | Jun | Jul | Aug | Sep | Okt | Nov | Dez |
|---|---|---|---|---|---|---|---|---|---|---|---|---|
| 0°N | 425 | 439 | 444 | 433 | 408 | 393 | 399 | 419 | 433 | 436 | 427 | 419 |
| 10°N | 374 | 402 | 433 | 444 | 439 | 433 | 433 | 439 | 433 | 416 | 385 | 365 |
| 30°N | 249 | 303 | 371 | 430 | 467 | 481 | 475 | 444 | 393 | 328 | 269 | 235 |
| 40°N | 181 | 243 | 323 | 405 | 464 | 490 | 473 | 430 | 354 | 272 | 198 | 161 |
| 46°N | 135 | 198 | 289 | 382 | 452 | 483 | 467 | 409 | 324 | 230 | 153 | 117 |
| 47°N | 128 | 191 | 283 | 378 | 450 | 482 | 466 | 406 | 319 | 224 | 146 | 110 |
| 48°N | 121 | 184 | 277 | 375 | 449 | 482 | 465 | 403 | 314 | 217 | 139 | 103 |
| 49°N | 114 | 177 | 271 | 371 | 447 | 481 | 464 | 400 | 309 | 211 | 132 | 96 |
| 50°N | 107 | 170 | 265 | 367 | 445 | 481 | 463 | 398 | 304 | 204 | 125 | 89 |
| 51°N | 100 | 163 | 259 | 363 | 443 | 480 | 462 | 394 | 298 | 197 | 118 | 83 |
| 52°N | 93 | 156 | 253 | 358 | 441 | 480 | 461 | 391 | 293 | 191 | 111 | 76 |
| 53°N | 86 | 149 | 247 | 354 | 439 | 479 | 459 | 388 | 287 | 184 | 104 | 70 |
| 54°N | 79 | 142 | 240 | 350 | 437 | 478 | 458 | 384 | 282 | 177 | 97 | 63 |
| 55°N | 73 | 135 | 234 | 345 | 435 | 478 | 457 | 381 | 276 | 170 | 90 | 56 |

The wind function f(v) of the Penman formula is written as

$$f(v) = 0.13 + 0.14 \cdot v \tag{8.6}$$

with v being the wind speed measured at 2 m above ground level. If there is no wind speed data measured in 2 m above ground available it can be corrected with

$$v_{corrected} = v_{recorded} \cdot (2/x)^{\frac{1}{7}} \tag{8.7}$$

where $v_{corrected}$ is the adjusted wind speed, $v_{recorded}$ the measured wind speed and x the height above ground the wind speed has been recorded.

# 9 Appendix 2

## IDL script for recharge flow:

```
; calculation of recharge (m/tstep)

; depending on the hydraulic conductivity at the water table

if approach eq "pow" then begin

;IF KEYWORD_SET(const_k) THEN BEGIN

;recharge = ((Sun_temp/Smaxun_temp)^soil.c * const_k)

;endif else begin

; power law depth of k

if soil.model eq 'pow' then recharge = ((Sun_temp/Smaxun_temp)^soil.c *
soil.ko*tstep*(1-(soil.D-wattab_s_temp)/soil.D)^(soil.m-1))

; exponential depth of k

if soil.model eq 'exp' then recharge = ((Sun_temp/Smaxun_temp)^soil.c *
(soil.ko*tstep*exp(-(soil.D-wattab_s_temp)/(soil.m))+soil.kc*tstep))

;endelse

endif

if approach eq "tt" then begin

recharge = (Sun_temp *
(1-exp(-soil.ko*tstep*Sun_temp/(soil.D-wattab_s_temp)^2*(Sun_temp/Smaxun_temp)^soil.c)))

endif

; no recharge if soil is saturated
```

```
wosat=where(Smaxun_temp eq 0, count_wosat)

wounsat=where(Smaxun_temp gt 0, count_wounsat)

wo_norecharge=where(noflow ne 0 or channel ne 0 or Sun_temp eq 0.0, count_norecharge)

if count_norecharge gt 0 then recharge(wo_norecharge)=0

wo_too_much = where(recharge gt Sun_temp, count_wo_too_much)

if count_wo_too_much gt 0 then recharge(wo_too_much) = Sun_temp(wo_too_much)

; total recharge per time step (m/tstep)

t.recharge(tt)=mean(recharge(wo_rain))
```

# 10 Appendix 3

## IDL script for bypass flow:

```
; calculation of bypass flow
;*********************************************************************

if min(soil.bypass) ne -99 then begin

; based on water content of unsaturated zone

if bypass_model eq "soil" then bypass(wo_rain) = infiltration*
(sun_temp(wo_rain)/smaxun_temp(wo_rain))^soil.bypass(wo_rain)

; based on rainfall intensity (or threshold?)

if bypass_model eq "precip" then begin

if infiltration le thres*tstep then begin

bypass(wo_rain) = infiltration* (infiltration/(thres*tstep))^soil.bypass(wo_rain) endif else begin
bypass(wo_rain)=bypass(wo_rain)+infiltration

endelse endif

; constant fraction of rainfall

if bypass_model eq "fraction" then bypass(wo_rain) = infiltration*thres*
(sun_temp(wo_rain)/smaxun_temp(wo_rain))^soil.bypass(wo_rain)

;bypass kann nicht grösser als infiltration sein

wo_too_much = where(bypass gt infiltration, count)

if count gt 0 then bypass(wo_too_much) = infiltration(wo_too_much)

;if saturation then no bypass flow if count_wosat gt 0 then bypass(wosat)=0.0

t.bypass(tt)=mean(bypass(wo_rain))

endif
```

# 11 Appendix 4

## IDL script for evapotranspiration routine:

```
;actual evapotranspiration

;evapo(wo_rain)=et(tt) ; Epot = Eact

;calculate et as fixed value or based on time series, Berechnung hier wie bei McGuire 2007!!!

if et(tt) gt 0 then begin

if count_wounsat gt 0 then begin

evapo(wounsat)=et(tt)*Sun_temp(wounsat)/Smaxun_temp(wounsat)

endif

wo_too_much = where (evapo gt et(tt),count)

if count gt 0 then evapo(wo_too_much) = et(tt)

if count_wosat gt 0 then evapo(wosat)=et(tt)

endif

t.evapo(tt)=mean(evapo(wo_rain))
```

# 12 Appendix 5

## IDL script for the snow routine:

```
;Snowmelt ;*************************************************************************

if t.tmp(tt) le 0 then begin ;beginnt wenn Temperaturzeitreihe unter 0 Grad Celsius

refr=RF*ddf*(Tm-t.tmp(tt))/1000 ;refreezing of retained liquid water

if refr lt RLW and RLW gt 0 then begin

RLW=RLW-refr;

SWE=SWE + t.precip(tt) + refr

StripSnowMelt=0

endif else if refr ge RLW and RLW gt 0 then begin

RLW=0;

SWE=SWE + t.precip(tt) + RLW

StripSnowMelt=0;

endif else if RLW eq 0 then begin

RLW=0;

SWE=SWE + t.precip(tt)

StripSnowMelt=0;

endif endif

if t.tmp(tt) gt 0 then begin

melt=ddf*(t.tmp(tt)-Tm)/1000 ;snow melt
```

```
if (melt lt SWE) and (SWE gt 0) then begin

SWE=SWE-melt;

RLW=RLW + t.precip(tt) + melt

LWRC=HC*SWE ; amount of water which can be retained in the snowpack

if RLW gt LWRC then begin

StripSnowMelt=RLW - LWRC;

RLW = LWRC;

endif endif else if (melt ge SWE) and (SWE gt 0) then begin

StripSnowMelt=RLW+ t.precip(tt) + SWE

SWE=0;

RLW=0;

endif else if SWE eq 0 then begin

SWE=0;

RLW=0;

StripSnowMelt = t.precip(tt) ;no Snow, all the precipitation as rain

endif

endif
```

# 13 Appendix 6

## IDL script for the calculation of water balance in unsaturated and saturated zone:

; water balance within each grid cell

; water change balance per grid cell

balance = dblarr(xx,yy)

wo_less = where(evapo le Sun_temp)

balance(wo_less) = recharge(wo_less) + bypass(wo_less) + ssf(wo_less)/siz^2

wo_more = where(evapo gt Sun_temp, count)

if count gt 0 then balance(wo_more) = recharge(wo_more) + bypass(wo_more) + ssf(wo_more)/siz^2 - (evapo(wo_more) - Sun_temp(wo_more))

;Anteil von evapo, der auf gesättigte Zone wirkt, wird von evapo abgezogen

if count gt 0 then evapo(wo_more) = Sun_temp(wo_more)

; potential storage in each cell until saturation

maxsat=soil.no*soil.b*(exp(-minunsat/soil.b)-exp(-(soil.D-wattab_s_temp)/soil.b)) ;+ (Smaxun-Sun) ;+ (soil.no*soil.b*(1-exp(-(minunsat)/soil.b)))

;infinitive values woinfinite = WHERE(FINITE(maxsat) EQ 0, count) if count gt 0 then maxsat(woinfinite)=0.0

;how to deal with watertable below subsur?

wo_negative=where(maxsat le 0.0, count) if count gt 0 then maxsat(wo_negative)=0.0

no_sat=where(balance lt maxsat and noflow eq 0 and channel eq 0, count_no_sat)

```
wo_sat=where(balance ge maxsat and noflow eq 0 and channel eq 0, count_wo_sat)

if count_wo_sat gt 0 then begin

wattab_s(wo_sat)=sur(wo_sat)-subsur(wo_sat) - minunsat

overland(wo_sat)=balance(wo_sat) - maxsat(wo_sat)

wo_greater = where(overland gt (Smaxun_temp - Sun_temp) and (Smaxun_temp - Sun_temp) gt 0, count)

if count gt 0 then overland(wo_greater) = overland(wo_greater) -
(Smaxun_temp(wo_greater)-Sun_temp(wo_greater))

if count gt 0 then Sun_temp(wo_greater) = Smaxun_temp(wo_greater)

wo_smaller = where(overland le (Smaxun_temp - Sun_temp) and (Smaxun_temp - Sun_temp) gt 0, count)

if count gt 0 then overland(wo_smaller) = 0.0

if count gt 0 then Sun_temp(wo_smaller) = Sun_temp(wo_smaller) + overland(wo_smaller)

endif

if count_no_sat gt 0 then begin

wattab_s(no_sat) =
soil.D(no_sat)-(-soil.b(no_sat)*alog((balance(no_sat))/(soil.no(no_sat)*soil.b(no_sat)) $
+exp(-(soil.D(no_sat)-wattab_s_temp(no_sat))/soil.b(no_sat))))

overland(no_sat)=0.0

endif

; infinitive values

woinfinite = WHERE(FINITE(wattab_s) EQ 0, count)

if count gt 0 then wattab_s(woinfinite)=0.0

;how to deal with watertable below subsur?

wo_below=where(wattab_s le 0.01, count)

if count gt 0 then wattab_s(wo_below)=0.01
```

# *13 Appendix 6*

;how to deal with watertable above sur?

wo_above=where(wattab_s gt (soil.d-minunsat), count)

if count gt 0 then wattab_s(wo_above)=(soil.d(wo_above)-minunsat)

deltaw(wo_rain)=wattab_s(wo_rain)-wattab_s_temp(wo_rain) ; water table fluctuation

Sun(wo_rain)=Sun_temp(wo_rain) + (infiltration(wo_rain)-bypass(wo_rain)) - recharge(wo_rain) - evapo(wo_rain) - (deltaw(wo_rain))*(soil.n(wo_rain)-(soil.no(wo_rain)*(exp(-(soil.D(wo_rain)-wattab_s_temp(wo_rain))/soil.b(wo_rain)))))

Smaxun(wo_rain) = soil.n(wo_rain)*(soil.D(wo_rain)-wattab_s(wo_rain))-soil.no(wo_rain)*soil.b(wo_rain)*(1-exp(-(soil.D(wo_rain)-wattab_s(wo_rain))/soil.b(wo_rain)))

wozero=where(Sun le 0.0, count) if count gt 0 then sun(wozero)=0.0

# 14 Appendix 7

## IDL script for the calculation of isotopic compositions in each flow process and for mixing in saturated and unsaturated storage:

### Recharge:

```
; isotope flux in recharge

if mass01 eq 1 then begin

; isotope flux depending on actual average isotope concentration in unsat zone

mass.recharge(wo_rain)=mass_un_temp(wo_rain)

woinfinite=where(finite(mass.recharge) eq 0, count)

if count gt 0 then mass.recharge(woinfinite)=0.0

tmass.recharge(tt)=mean(mass.recharge(wo_rain))

endif
```

### Bypass flow:

```
;isotope flux in bypass

if mass01 eq 1 then begin

; concentration from precipitation

mass.bypass(wo_rain)=o18precip(tt)

woinfinite=where(finite(mass.bypass) eq 0, count)

if count gt 0 then mass.bypass(woinfinite)=0.0

tmass.bypass(tt)=mean(mass.bypass(wo_rain))

endif
```

## Saturated Subsurface Flow:

;isotope flux in saturated zone

if mass01 eq 1 then begin

flux_mm = flux/siz^2

;Wenn kein flux soll trotzdem nicht Isotopenzusammensetzung = 0.0

wo_zero = where(flux_mm le 0.0, count_zero)

if count_zero gt 0 then flux_mm(wo_zero) = 0.0000001

case i of

0:mass.ssf(1:xx-2,2:yy-1)=((flux_mm)/(sat(1:xx-2,2:yy-1)+(flux_mm)))*mass_sat_temp(1:xx-2,1:yy-2)+(sat(1:xx-2,2:yy-1)/(sat(1:xx-2,2:yy-1)+(flux_mm)))*mass_sat_temp(1:xx-2,2:yy-1)
1:mass.ssf(1:xx-2,0:yy-3)=((flux_mm)/(sat(1:xx-2,0:yy-3)+(flux_mm)))*mass_sat_temp(1:xx-2,1:yy-2)+(sat(1:xx-2,0:yy-3)/(sat(1:xx-2,0:yy-3)+(flux_mm)))*mass_sat_temp(1:xx-2,0:yy-3)
2:mass.ssf(0:xx-3,1:yy-2)=((flux_mm)/(sat(0:xx-3,1:yy-2)+(flux_mm)))*mass_sat_temp(1:xx-2,1:yy-2)+(sat(0:xx-3,1:yy-2)/(sat(0:xx-3,1:yy-2)+(flux_mm)))*mass_sat_temp(0:xx-3,1:yy-2)
3:mass.ssf(2:xx-1,1:yy-2)=((flux_mm)/(sat(2:xx-1,1:yy-2)+(flux_mm)))*mass_sat_temp(1:xx-2,1:yy-2)+(sat(2:xx-1,1:yy-2)/(sat(2:xx-1,1:yy-2)+(flux_mm)))*mass_sat_temp(2:xx-1,1:yy-2)
4:mass.ssf(2:xx-1,2:yy-1)=((flux_mm)/(sat(2:xx-1,2:yy-1)+(flux_mm)))*mass_sat_temp(1:xx-2,1:yy-2)+(sat(2:xx-1,2:yy-1)/(sat(2:xx-1,2:yy-1)+(flux_mm)))*mass_sat_temp(2:xx-1,2:yy-1)
5:mass.ssf(0:xx-3,0:yy-3)=((flux_mm)/(sat(0:xx-3,0:yy-3)+(flux_mm)))*mass_sat_temp(1:xx-2,1:yy-2)+(sat(0:xx-3,0:yy-3)/(sat(0:xx-3,0:yy-3)+(flux_mm)))*mass_sat_temp(0:xx-3,0:yy-3)
6:mass.ssf(0:xx-3,2:yy-1)=((flux_mm)/(sat(0:xx-3,2:yy-1)+(flux_mm)))*mass_sat_temp(1:xx-2,1:yy-2)+(sat(0:xx-3,2:yy-1)/(sat(0:xx-3,2:yy-1)+(flux_mm)))*mass_sat_temp(0:xx-3,2:yy-1)
7:mass.ssf(2:xx-1,0:yy-3)=((flux_mm)/(sat(2:xx-1,0:yy-3)+(flux_mm)))*mass_sat_temp(1:xx-2,1:yy-2)+(sat(2:xx-1,0:yy-3)/(sat(2:xx-1,0:yy-3)+(flux_mm)))*mass_sat_temp(2:xx-1,0:yy-3)

endcase

endif

## Falling and rising water table:

```
if mass01 eq 1 then begin

;mass exchange due to falling and rising water table ;

wodeltaw_plus = where(deltaw ge 0.0, count) ;rising watertable

if count gt 0 then begin

mass.delta(wodeltaw_plus)=mass_sat_temp(wodeltaw_plus)

endif

wodeltaw_minus = where(deltaw lt 0.0, count_wodeltaw_minus)

if count_wodeltaw_minus gt 0 then begin

mass.delta(wodeltaw_minus)=mass_sat_temp(wodeltaw_minus)

endif

woinfinite=where(finite(mass.delta) eq 0, count)

if count gt 0 then mass.delta(woinfinite)=0.0
```

## Mixing in unsaturated zone:

```
;Unsat

Menge1_un=dblarr(xx,yy)

Menge2_un=dblarr(xx,yy)

Menge3_un=dblarr(xx,yy)

Menge1_un(wo_rain) = Sun(wo_rain)

;Wenn Zelle leer, soll sie trotzdem nicht Isotopenzusammensetzung = 0.0 erhalten:

wo_zero = where(Menge1_un le 0.0, count_zero)

if count_zero gt 0 then Menge1_un(wo_zero) = 0.0000001

Menge2_un(wo_rain) = infiltration(wo_rain) - bypass(wo_rain)
```

```
if count_wodeltaw_minus gt 0 then begin

Menge3_un(wodeltaw_minus) = -
(deltaw(wodeltaw_minus))*(soil.n(wodeltaw_minus)-(soil.no(wodeltaw_minus)*(exp(-
(soil.D(wodeltaw_minus)-wattab_s_temp(wodeltaw_minus))/soil.b(wodeltaw_minus)))))

endif

mass.un=(Menge1_un/(Menge1_un+Menge2_un+Menge3_un))*mass_un_temp +
(Menge2_un/(Menge1_un+Menge2_un+Menge3_un))*mass.infiltration +
(Menge3_un/(Menge1_un+Menge2_un+Menge3_un))*mass.delta
```

## Mixing in saturated zone:

```
;Sat

Menge_sat=dblarr(xx,yy)

sat = dblarr(xx,yy)

sat_temp = dblarr(xx,yy)

sat = wattab_s * soil.n sat_temp = wattab_s_temp*soil.n

wo_plus = where(ssf ge 0.0 and deltaw ge 0.0, count)

if count gt 0 then begin Menge_sat(wo_plus)=sat_temp(wo_plus)+recharge(wo_plus)+bypass(wo_plus)+ssf(wo_plus)/siz^2+

(deltaw(wo_plus))*(soil.n(wo_plus)-(soil.no(wo_plus)*(exp(-(soil.D(wo_plus)-

wattab_s_temp(wo_plus))/soil.b(wo_plus)))))

mass.sat(wo_plus)=(sat_temp(wo_plus)/Menge_sat(wo_plus))*mass_sat_temp(wo_plus)+

(recharge(wo_plus)/Menge_sat(wo_plus))*mass.recharge(wo_plus)$
+(bypass(wo_plus)/Menge_sat(wo_plus))*mass.bypass(wo_plus)+

((ssf(wo_plus)/siz^2)/Menge_sat(wo_plus))*mass.ssf(wo_plus)$ +

((deltaw(wo_plus))*(soil.n(wo_plus)-(soil.no(wo_plus)*(exp(-(soil.D(wo_plus)-

wattab_s_temp(wo_plus))/soil.b(wo_plus)))))$ /Menge_sat(wo_plus))*mass_un_temp(wo_plus)

endif
```

```
wo_ssf_plus = where(ssf ge 0.0 and deltaw lt 0.0, count)

if count gt 0 then begin

Menge_sat(wo_ssf_plus)=sat_temp(wo_ssf_plus)+recharge(wo_ssf_plus)+bypass(wo_ssf_plus)+ssf(wo_ssf_plus)/siz^2

mass.sat(wo_ssf_plus)=(sat_temp(wo_ssf_plus)/Menge_sat(wo_ssf_plus))*mass_sat_temp(wo_ssf_plus)+

(recharge(wo_ssf_plus)/Menge_sat(wo_ssf_plus))*mass.recharge(wo_ssf_plus)$
+(bypass(wo_ssf_plus)/Menge_sat(wo_ssf_plus))*mass.bypass(wo_ssf_plus)+

((ssf(wo_ssf_plus)/siz^2)/Menge_sat(wo_ssf_plus))*mass.ssf(wo_ssf_plus)

endif
```

# 15 Appendix 8

## IDL script for the calculation of the isotopic composition of snowmelt:

```
; isotope flux in infiltration

if mass01 eq 1 then begin

; isotope flux depending on actual average isotope concentration in precipitation

;um Isotopengehalt von Schneeschmelze als Anteil der infiltration zu berücksichtigen

if swe gt 0.0 then begin what_o18 = min(where(t.swe_current gt 0.0))

if t.precip(tt) gt 0.0 then mass.infiltration(wo_rain)=mean(o18precip(what_o18:tt))

if t.precip(tt) eq 0.0 then mass.infiltration(wo_rain)=o18precip(what_o18)

endif else begin

mass.infiltration(wo_rain)=o18precip(tt)

endelse

woinfinite=where(finite(mass.recharge) eq 0, count)

if count gt 0 then mass.infiltration(woinfinite)=0.0

tmass.infiltration(tt)=mean(mass.infiltration(wo_rain))

endif
```

# Ehrenwörtliche Erklärung

Hiermit erkläre ich, dass die Arbeit selbständig und nur unter Verwendung der angegebenen Hilfsmittel angefertigt wurde.

Ort, Datum Unterschrift